USGS
science for a changing world

Aeromagnetic Map of Northeastern California

By Victoria E. Langenheim and Donald S. Sweetkind

Pamphlet to accompany
Scientific Investigations Map 3505

2023

U.S. Department of the Interior
U.S. Geological Survey

U.S. Geological Survey, Reston, Virginia: 2023

For more information on the USGS—the Federal source for science about the Earth, its natural and living resources, natural hazards, and the environment—visit https://www.usgs.gov or call 1–888–ASK–USGS.

For an overview of USGS information products, including maps, imagery, and publications, visit https://store.usgs.gov.

Suggested citation:
Langenheim, V.E. and Sweetkind, D.S., 2023, Aeromagnetic map of northeastern California: U.S. Geological Survey Scientific Investigations Map 3505, pamphlet 21 p., https://doi.org/10.3133/sim3505.

Associated data for this publication:
Langenheim, V.E., 2022, Aeromagnetic Data of Alturas, California, and Surrounding Areas: U.S. Geological Survey data release, https://doi.org/10.5066/P9LU37RC.

Langenheim, V.E., 2023, Aeromagnetic and derivative gridded data, and magnetization boundaries of northeastern California: U.S. Geological data release, https://doi.org/10.5066/P9PUFYDD.

Sweetkind, D.S., and Langenheim, V.E., 2022, Data release of geologic data for the aeromagnetic map of northeastern California: U.S. Geological Survey data release, https://doi.org/10.5066/P91Y9L0H.

ISSN 2331-1258 (online)

Cover. Photograph of the west central part of the map area, looking east-northeast from the Soldier Mountain fire lookout, about 23 kilometers (km) northeast of Burney, California. Grassy low terrain in the center of photo is the Fall River Valley, underlain by young alluvial deposits and diatomite. Low, tree-covered terrain at left-center is in part underlain by the southern end of the 45-km long, 12.5 kilo-annum (ka) basalt of Giant Crater associated with the Medicine Lake volcano and in part underlain by the Brushy Butte flow field, consisting of tholeiitic basalt erupted about 35.7 Ka. These volcanic rocks conduct much of the groundwater the emerges at the Fall River spring discharge area, a 16 km wide zone near the southern terminus of the basalt of Giant Crater lava Flow. This spring discharge is the source of the broad Tule River at right-center and the meandering Fall River at center, which themselves are the predominant source of water to the Pit River to the south (right) of the photo. On the center skyline are the Big Valley Mountains, underlain by Pliocene to Miocene andesitic volcanic rocks. U.S. Geological Survey photograph taken by Donald S. Sweetkind, June 2019.

Acknowledgments

The U.S. Geological Survey National Cooperative Geologic Mapping program and the Bureau of Land Management provided funding for this study. We thank Michael Hobbs and the rest of the crew at Edcon-PRJ., Inc., who flew the Alturas survey and processed the data to total-field anomalies. We thank the Northern California Earthquake Data Center for data access. Joseph Colgan and Jonathan Glen provided constructive reviews and Mitchell Phillips provided a skilled edit.

Contents

Figures

Conversion Factors

U.S. customary units to International System of Units

Multiply	By	To obtain
Length		
foot (ft)	0.3048	meter (m)
mile (mi)	1.609	kilometer (km)

Abbreviations

GIS	geographic information system
GPS	Global Positioning System
M	magnitude
Ma	mega-annum (a unit of time equivalent to one million years)
PDF	portable document file
USGS	U.S. Geological Survey

Aeromagnetic Map of Northeastern California

By Victoria E. Langenheim and Donald S. Sweetkind

Abstract

Aeromagnetic surveys were conducted to improve understanding of the geology and structure in northeastern California, a region predominantly covered by Quaternary and Tertiary, mainly Neogene, volcanic rocks including Medicine Lake volcano. New aeromagnetic data are a substantial improvement over existing data and reveal structural details not resolved by older surveys. Here we show how these data (1) do not support the presence of a northwest-striking structural feature across the Modoc Plateau, (2) reveal a northeast-striking fault-bounded block of predominantly reversely magnetized material that may influence tectonism at Medicine Lake volcano, and (3) constrain possible right-lateral offsets along the Likely Fault Zone and other faults that traverse the region. The data also highlight possible extensions of mapped faults, such as those in Fall River Valley and the Tule and Lower Klamath Lake areas.

Introduction

Aeromagnetic surveys were conducted to promote further understanding of the geology and structure in northeastern California, and to serve as a basis for geophysical interpretations, geologic mapping, water and geothermal resource investigations, and volcanic and seismic hazard assessments. This study presents a continuous detailed aeromagnetic dataset that covers roughly 27,300 square kilometers (km^2) in northeastern California, merging the Burney aeromagnetic survey flown in 2017 with the Alturas aeromagnetic survey flown in 2019. Here we refine the preliminary results of the Burney aeromagnetic survey (Langenheim, 2021) and add discussion of magnetic anomalies to the north and east (figs. 1, 2).

The study area lies at or near the intersection of multiple geologic provinces in northern California (fig. 1; Langenheim and others, 2016). The aeromagnetic surveys cover the southern part of the Quaternary Cascade arc as well as the poorly delineated southern end of the Oregon coast block (Unruh and Humphrey, 2017). The surveys also extend across the westernmost part of the extensional Basin and Range geologic province where it abuts the Modoc Plateau, a large region of remarkably low relief covered by numerous thin basalt flows offset by normal faults. Duffield and Fournier (1974) proposed a northwest-trending lineament across the plateau connecting volcanoes at Round Mountain and Blue Mountain and parallel to the Likely Fault Zone (fig. 2), which may have right-lateral offset. The Walker Lane tectonic province, a zone of right-lateral shear east of the Sierra Nevada–Great Valley block, encroaches into the survey area, perhaps as far west as Medicine Lake volcano where focal mechanisms and GPS data indicate a component of right-lateral shear (Poland and others, 2006). The amount of right-lateral offset for the shear zone is unknown in this area, although faults in the northern Walker Lane tectonic province have potentially accommodated as much as 30 kilometers (km) of displacement (Wesnousky, 2005; Faulds and others, 2005). Existing aeromagnetic data before these surveys lack sufficient resolution to quantify the amount of right-lateral offset along northwest-striking faults in this region.

Areally extensive volcanic rocks of mostly Tertiary and Quaternary age blanket the study area and are locally overlain by sedimentary deposits of a similar age (fig. 3; Jennings and others, 2010). The volcanic rocks are of both tholeiitic and calc-alkaline affinities, reflecting the influence of Basin and Range extension and Cascade subduction zone in this area (Clynne and Muffler, 2017). However, much of the existing geologic mapping (Gay and Aune, 1958), except for Medicine Lake and Lassen volcanoes (Donnelly-Nolan, 2011; Clynne and Muffler, 2010), predates the advent of radiometric dating and paleomagnetic studies, critical for differentiating individual flows or volcanic centers. Although geologic maps of the Cedarville, Alturas, Susanville, and Eagle Lake 1:100,000-scale quadrangles (Grose and others, 2014a, b; Grose and others, 2016, 2017) in the eastern part of the study area include geochronology and are a substantial improvement over older mapping, these maps are preliminary and do not include paleomagnetic analyses. Many of the basalt flows share similar geochemistry; thus, paleomagnetic data provide a way to differentiate flows whereas aeromagnetic data may aid in determination of polarity, particularly for volcanic edifices. Given that the survey area is blanketed by Tertiary and Quaternary volcanic rocks, with basement outcrops limited to the eastern part of the Klamath Mountains and near Eagle Lake (fig. 3), the aeromagnetic data may provide insight into not only the distribution of volcanic units but also the subvolcanic geologic framework.

The aeromagnetic data described here support a variety of resource and hazards investigations. Although this area is sparsely populated, it includes Medicine Lake volcano and its

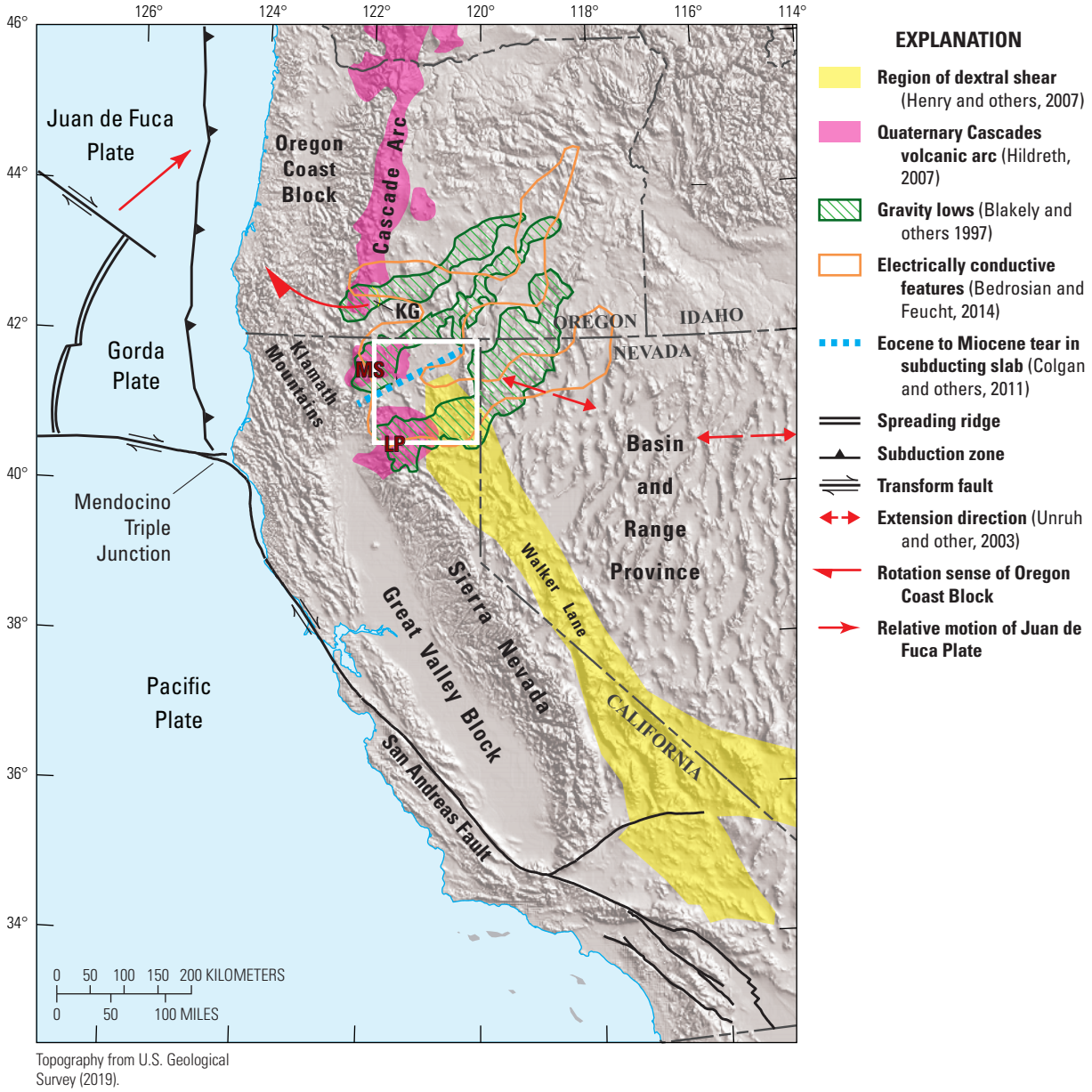

Figure 1. Shaded-relief topographic map showing major tectonic and geophysical features of the study area (outlined in white and shown in figures 2–6). KG, Klamath Graben; LP, Lassen Peak; MS, Mount Shasta.

surrounding highlands, considered to be the main recharge region for some of the largest fresh-water springs in the United States (fig. 2; Meinzer, 1927). These springs contribute more than 50 percent of the Pit River perennial flow (Davisson and Rose, 2014), which is the largest tributary to Shasta Lake, the largest reservoir in California. The Pit River is also a substantial tributary of the Sacramento River, which is the largest and longest river in the state. These numerous springs are located near the terminus of laterally extensive lava flows, indicating that these volcanic units host important groundwater systems. Aeromagnetic data offer a potentially important tool for hydrologic studies in this area because they can help map subsurface geology, given that volcanic rocks are strongly magnetic.

Medicine Lake volcano has also been a target for geothermal exploration. Although surface evidence of a geothermal system, such as fumaroles or hydrothermal alteration, is limited (Donnelly Nolan, 2010), exploratory drilling initiated in the 1980s encountered alteration and temperatures that indicate a high-temperature geothermal system in the caldera (Hulen and Lutz, 1999). A variety of geophysical observation methods have been employed to characterize the geothermal system and the underpinnings of Medicine Lake volcano, including gravity (Finn and Williams, 1982), seismic tomography (Evans and Zucca, 1988; Chiarabba and others, 1995), electric (Zohdy and Bisdorf, 1990; Cumming and Mackie, 2010), and inversion of aeromagnetic data (Wang

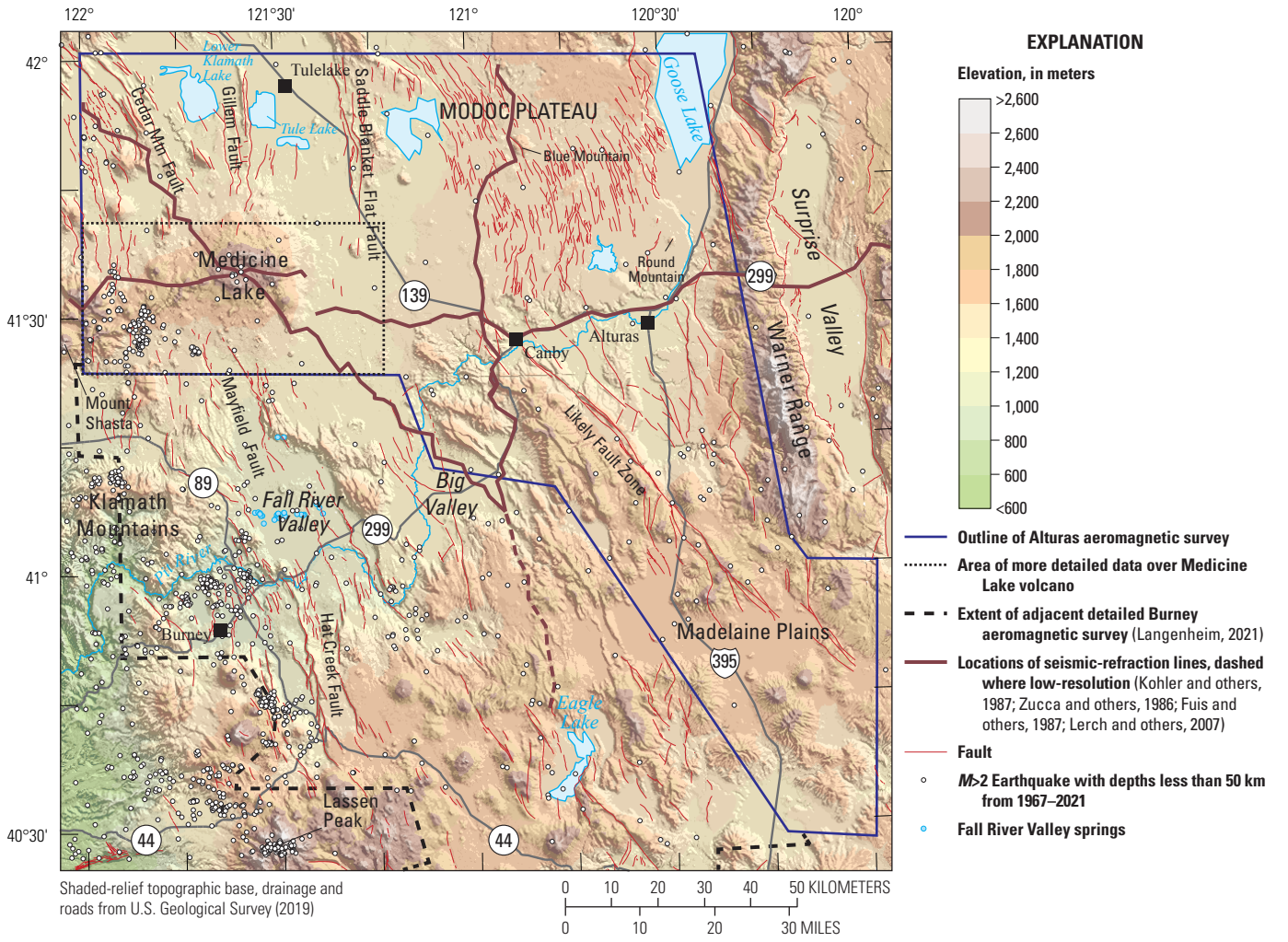

Figure 2. Shaded-relief topographic map of northeastern California (see figure 1 for reference). Earthquake data from Northern California Earthquake Data Center dataset (NCEDC, 2014). Fault locations from U.S. Geological Survey and California Geological Survey (2006). M, magnitude; Mtn, Mountain; km, kilometer.

and Hansen, 1990). Seismic-refraction and magnetotelluric profiles intended to probe the middle to lower crust also traverse the study area (fig. 2; Zucca and others, 1986; Fuis and others, 1987; Stanley and others, 1990). Aeromagnetic data can aid geothermal exploration by mapping structures that influence geothermal systems, such as faults and zones of alteration.

Seismic hazards are a concern in this area, as many of the Quaternary volcanic rocks, including the Hat Creek Basalt and the basalt of Giant Crater of Donnelly-Noland (2010), are offset by faults (figs. 2, 3). Despite the area's low population, substantial infrastructure, including dams along the Pit River, are at risk. Although seismicity is generally dispersed across the survey area, three historical earthquakes of about magnitude (*M)* 6.2 in the late 1800s between Honey and Eagle Lakes south of the study area produced widespread shaking (as much as Modified Mercalli Intensity 6; California Geological Survey, 2019) and earthquake swarms (as large as *M*4.6) have occurred near Medicine Lake volcano (fig. 2; Dzurisin and others, 1991). High-resolution aeromagnetic data can aid in mapping faults and providing information on cumulative offset (Glen and others, 2013).

Data

The Burney aeromagnetic survey acquisition is described by Langenheim (2021). The Alturas aeromagnetic survey (fig. 2) was flown over the entire Tule Lake and parts of the Alturas, Cedarville, Eagle Lake, and McArthur 1:100,000-scale quadrangles, totaling an area of approximately 14,124 km^2. Data-collection and -processing to total-field anomalies were carried out by EDCON-PRJ, Inc., under contract to the U.S. Geological Survey. Total-field aeromagnetic data were collected from September 24 to November 2, 2019, along east-west oriented flight lines, spaced 800 meters (m) apart, except over Medicine Lake volcano, where flight line spacing was 400 m (fig. 2). Distance between measurements along a flight line was about 8 m. North-south oriented tie lines were spaced 8,000 m apart (4,000 m for Medicine Lake area). The specified survey height of the aircraft above the ground was 305 m, close to the average height of the aircraft of approximately 312 m ± 30 m (fig. 4). Locally, the aircraft was flown higher than 305 m because of safety considerations owing to steep slopes, for example those

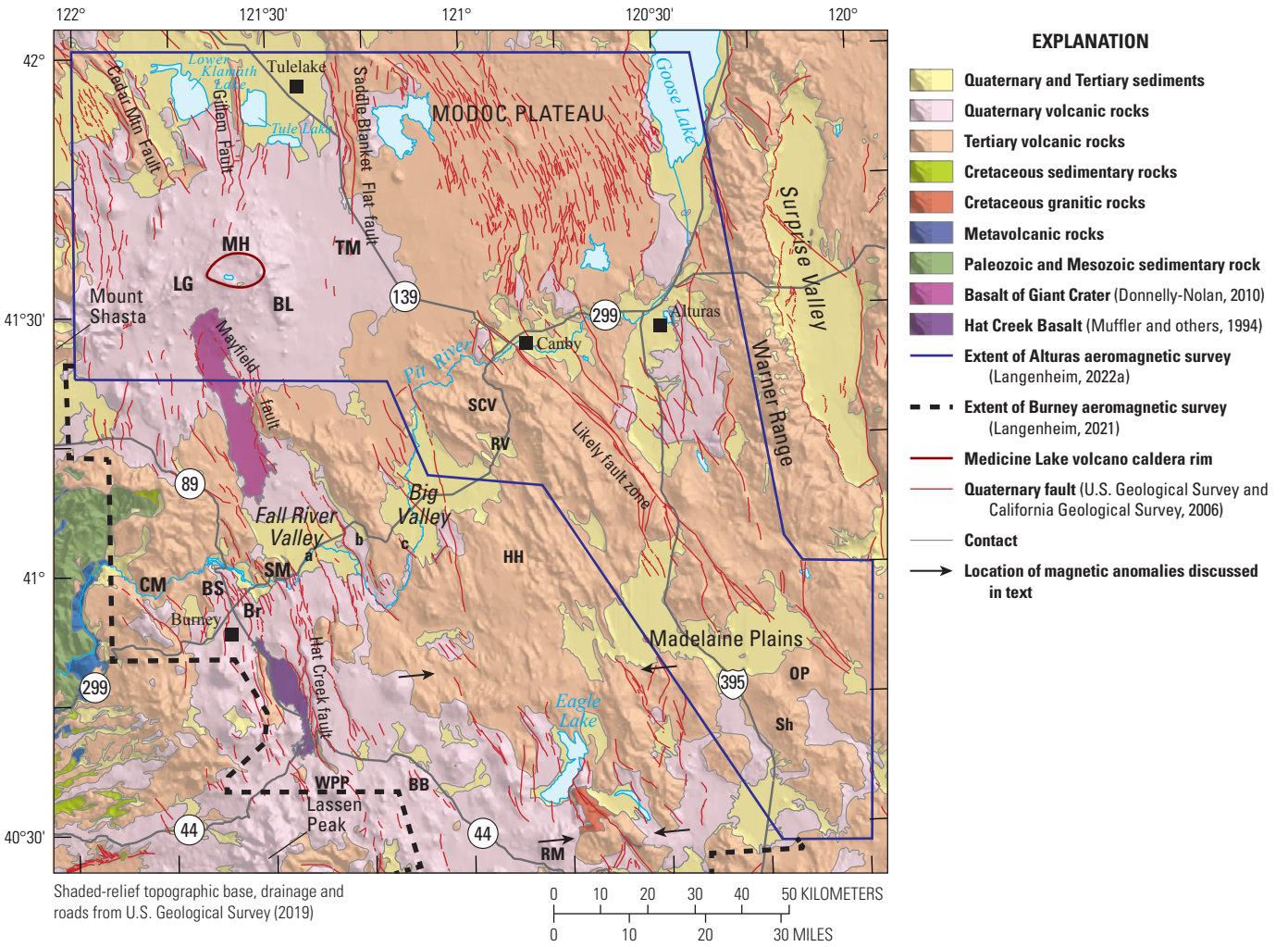

Figure 3. Simplified geologic map of northeastern California (modified from Jennings and others, 2010). Arrows point to linear anomalies that are not disrupted by strike-slip offset and a, b, and c refer to locations of semicircular magnetic anomalies discussed in Langenheim (2021). Geographic abbreviations: BB, Bogard Buttes; BL, Black Mountain, Br, Brush Mountain; BS, Burney Spring Mountain; CM, Chalk Mountain; HH, Hayden Hill; LG, Little Glass Mountain; MH, Mount Hoffman; OP, Observation Peak; RM, Roop Mountain; RV, Round Valley; SCV, Stone Coal Valley; Sh, Shinn Mountain; SM, Saddle Mountain; TM, Timber Mountain; WPP, West Prospect Peak. Mtn, Mountain.

forming Mount Dome, Observation Peak, Haight Mountain, and the foothills of the Warner Range (fig. 2). In the areas adjacent to steep slopes, anomalies are smoother because of the higher flight elevation. Note that the airplane in the Burney survey was generally flown higher (fig. 4) because of more rugged topography and weather conditions.

The aeromagnetic measurements of the Alturas survey (Langenheim, 2022) were collected using a cesium-vapor magnetometer (Geometrics G823A) mounted in the tail boom of the aircraft. Measurements were corrected for the magnetic effect of the airplane using a triaxial fluxgate magnetometer and performing magnetic compensation flights. The measurements were adjusted so that the resulting magnetic field shown in the map and in figure 5*B* is relatively free of artifacts owing to the plane itself. Data were adjusted for tail sensor lag and diurnal field variations. The base magnetometer used to correct the diurnal field variations was a Geometrics G-858 magnetometer located in magnetically quiet areas at the Klamath Falls and Susanville Municipal Airports (lat 42.170181° N., long 121.745744° W. and lat 40.377573° N., long 120.574954° W., respectively). Further processing included leveling using the tie lines, microleveling, and correction for the Earth's main magnetic field (International Geomagnetic Reference Field; see Langel, 1992), updated to the period during which the data were collected (September 24 to November 2, 2019).

The resulting data from the Alturas survey (Langenheim, 2022) were transformed to a Universal Transverse Mercator projection (base latitude, 0°; central meridian, −121° W) and interpolated to a square grid, using a grid interval of 200 m and the principle of minimum curvature (Briggs, 1974). Accuracy of these survey data is 1 nanotesla (nT) or better. The gridded data of the Alturas survey were combined with gridded data of the detailed Burney survey to the south by subtracting their respective, slightly adjusted, mean magnetic base levels to bring them onto a common magnetic datum, resulting in a single merged grid (Langenheim, 2023).

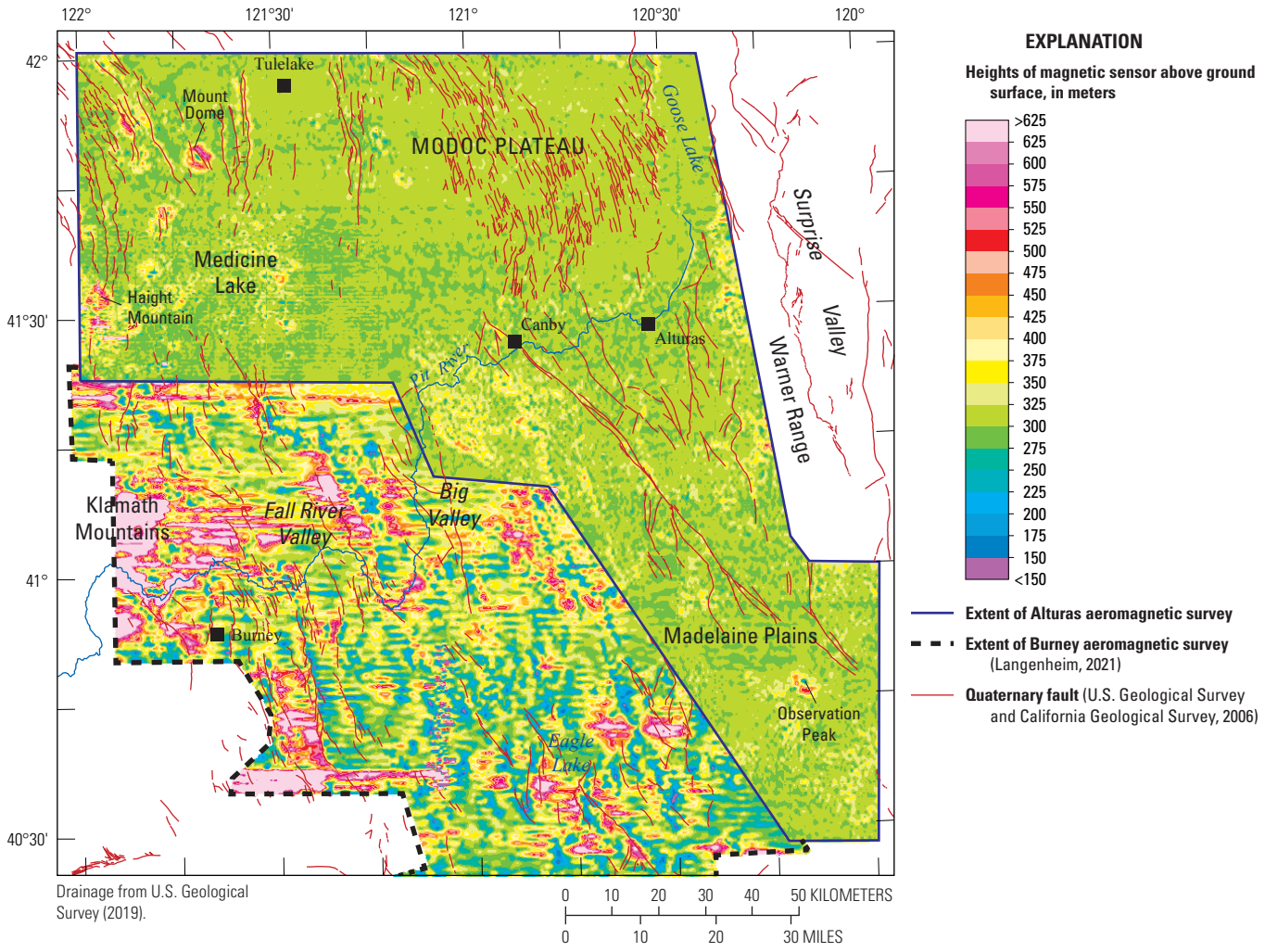

Figure 4. Map of Alturas survey showing heights of magnetic sensor above ground surface measured by radar altimetry and precise GPS positioning of the aircraft. Also shown are heights of magnetic sensor above ground surface measured by radar altimetry for the Burney survey to the southwest. Shaded relief map removed for clarity. Pit River course from U.S. Geological Survey (2019).

The new Alturas data provide a considerable improvement on older data (fig. 5*A*), which consisted of profiles flown 1.6 km apart at a constant altitude of 2,740 m (Couch and Gemperle, 1982). The 1982 dataset was collected at too high of an elevation over valley areas and much of the Modoc Plateau to measure short-wavelength anomalies associated with near-surface or exposed sources, such as volcanic rocks. Although aeromagnetic profiles were flown closer to the ground (120 m) by the National Uranium Resource Evaluation Program (Hill and others, 2009), these lines were flown too far apart (4,800 m) to effectively map the magnetic field between the lines. When compared with the older data (fig. 5*A*), the map from the current Alturas survey (fig. 5*B*), and Burney survey to the south, reveals substantially more short-wavelength magnetic anomalies, which are associated with Quaternary and Tertiary volcanic rocks. The magnetic expression of major Quaternary faults is substantially sharpened, for example, along the Cedar Mountain, Hat Creek, Gillem, Mayfield, and Saddle Blanket Flat Faults (figs. 2, 5*B*).

To aid in interpretation of the aeromagnetic data, geologic map data were compiled (Sweetkind and Langenheim, 2022) that focused on the existence and location of faults and volcanic features—geologic elements considered most likely to produce a magnetic anomaly. Faults, particularly those with documented Quaternary offset, affect the regional pattern of magnetic anomalies through juxtaposition of rocks with differing magnetic properties. Faults with interpreted Quaternary offset were compiled from the U.S. Geological Survey Quaternary fault and fold database without simplification or edits (U.S. Geological Survey and California Geological Survey, 2006). Faults with pre-Quaternary offset were compiled from 1:50,000-scale maps of Lassen Volcanic National Park and Medicine Lake volcano (Donnelly-Nolan, 2010; Muffler and others, 2010; Ramsey and others, 2010), from 1:100,000-scale mapping in the eastern half of the survey area (Grose, Saucedo, and Wagner, 2014a, b; Grose, Egger, and O'Neil 2016, 2017). Outside of these map areas, pre-Quaternary faults were compiled from the regional compilation of Sherrod and Keith (2018).

The location of volcanic vents is potentially useful to interpretation of the aeromagnetic data because vent alignments may indicate zones of crustal weakness and the potential

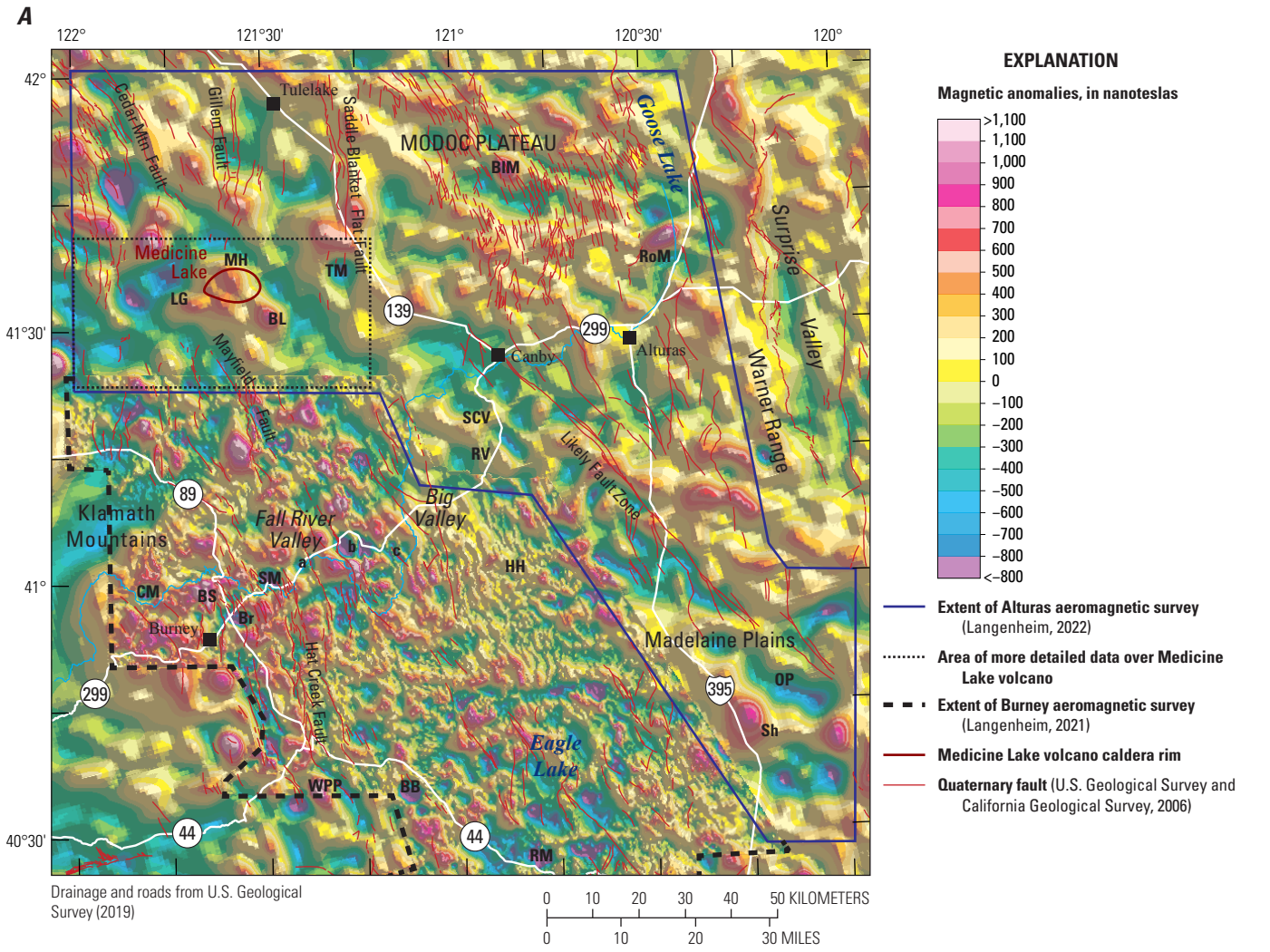

Figure 5. Colored shaded-relief-aeromagnetic maps of northeastern California. *A*, Aeromagnetic map based on previous surveys (North American Magnetic Anomaly Group, 2002) and the Burney survey (Langenheim, 2021). *B*, Aeromagnetic map based on data from the Alturas survey (Langenheim, 2023) merged with those of the Burney survey. Arrows point to linear anomalies that are not disrupted by strike-slip offset and a, b, and c refer to locations of semicircular magnetic anomalies discussed in Langenheim (2021). Geographic abbreviations: BB, Bogard Buttes; BL, Black Mountain, BIM, Blue Mountain; Br, Brush Mountain; BS, Burney Spring Mountain; CM, Chalk Mountain; HH, Hayden Hill; LG, Little Glass Mountain; MH, Mount Hoffman; OP, Observation Peak; RM, Roop Mountain; RoM, Round Mountain; RV, Round Valley; SCV, Stone Coal Valley; Sh, Shinn Mountain; SM, Saddle Mountain; TM, Timber Mountain; WPP, West Prospect Peak. Mtn, Mountain.

presence of magnetic anomaly sources deeper in the crust. The locations of volcanic vents were compiled primarily from Blakely and others (1997), augmented by data from published geologic maps in the study area (Donnelly-Nolan, 2010; Muffler and others, 2010; Ramsey and others, 2010; Grose, Saucedo, and Wagner, 2014a, b; Grose, Egger, and O'Neil 2016, 2017). Vent locations were confirmed through comparison with U.S. Geological Survey (USGS) seamless 1:24,000-scale National Elevation Data digital elevation models (https://www.usgs.gov/core-science-systems/ngp/tnm-delivery, accessed July 2022) and individual points were edited to eliminate duplication between the data sources.

Volcanic edifices with cone or shield geometry, predominantly of Miocene age and calc-alkaline composition, are a common element of the volcanic-rock sequences in the study area within the northern Walker Lane tectonic province and to the east of the modern Cascade arc (Guffanti and others, 1990; Grose, 2000; du Bray and John, 2009; Colgan and others, 2011). Generalized extent boundaries of these volcanoes in the eastern half of the survey area were compiled from 1:100,000-scale mapping (Grose, Saucedo, and Wagner, 2014a, b; Grose, Egger, and O'Neil 2016, 2017). In the western half of the study area, volcano boundaries were derived from several detailed geologic maps (McDonald, 1965; Donnelly-Nolan, 2010;

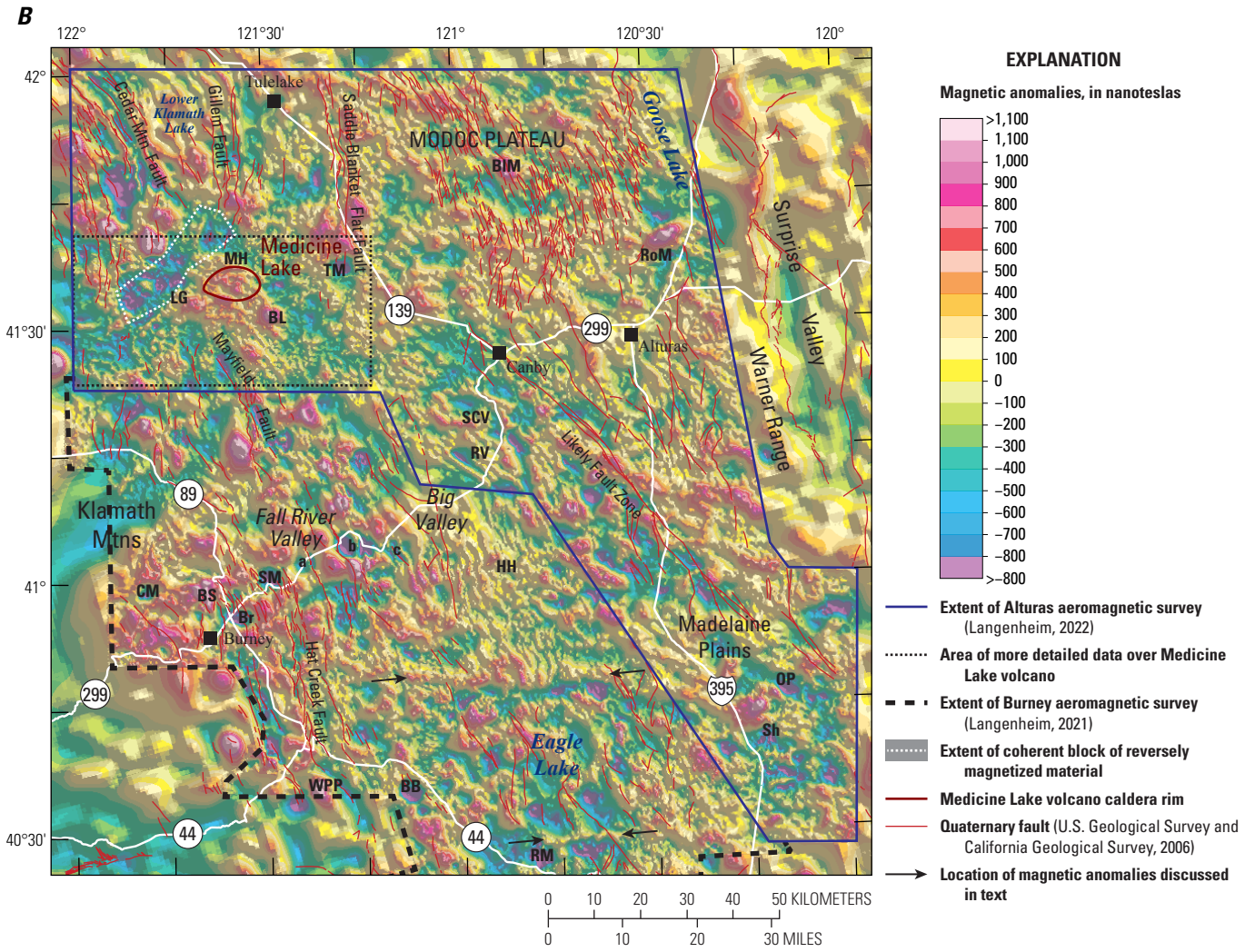

Figure 5. *Continued*

Muffler and others, 2010; Ramsey and others, 2010); locally mapped volcanic contacts from 1:250,000-scale geologic maps (Gay and Aune, 1958; Lydon and others, 1960) were compiled where a digital elevation model (https://www.usgs.gov/core-science-systems/ngp/tnm-delivery, accessed July 2022) showed features that were morphologically similar to volcanic edifices mapped in detail elsewhere in the study area.

The map area is largely covered by voluminous accumulations of Cenozoic volcanic rocks that originate from a variety of volcanic centers, span a wide age range, and are diverse both compositionally and in their extrusive structures (Luedke and Smith, 1981; Sherrod and Keith, 2018). Volcanic rocks in the mapped area can be broadly subdivided into (1) volcanic rocks derived from Pliocene to Quaternary volcanoes of the active arc and associated Pleistocene valley filling basaltic lava flows, and (2) deeply dissected Paleogene to Neogene (mostly Eocene to late Miocene) volcanoes of the ancestral Cascades arc, effusive late Miocene to Pliocene basalt lava flows erupted in an extensional back-arc setting, and diverse Cenozoic volcanic rocks erupted across the Basin and Range Province since the Eocene (Guffanti and others, 1990; Blakely and others, 1997; du Bray and others, 2009; Donnelly-Nolan, 2010; Muffler and others, 2010). Creating a geologic map layer that incorporates the previously described volcanic rock subdivisions would have required a new regional volcanic-rock geologic map compilation with several map units that was beyond the scope of the present study. Instead, geologic polygons were compiled from a digital GIS database of Cenozoic rocks in the Pacific Northwest (Sherrod and Keith, 2018). Map polygons were generalized into a small number of classes that could readily be shown at a scale of 1:250,000 in conjunction with the aeromagnetic data. We considered using some combination of the volcanic rock age, composition, and morphology attributes tabulated by Sherrod and Keith (2018) but opted instead for a first-order age-based subdivision that might assist with interpretation of the aeromagnetic data. Quaternary and Holocene volcanic rocks (map unit QHv in Description of Map Units) are assumed to be most influential in

influencing the shallowest magnetic anomaly patterns, whereas pre-Quaternary volcanic rocks (map unit Tvu in Description of Map Units), often buried by the younger volcanic rocks, might be assumed responsible for some of the deeper-seated anomalies. Quaternary deposits and shallowly buried sediments were combined into a single map unit (map unit QTs in Description of Map Units); these sediments and deposits likely have little effect on the magnetic character of the map area. Geologic polygons were locally edited so mapped contacts closed against the fault layers that were compiled (Sweetkind and Langenheim, 2022).

Interactive PDF

The geophysical and geologic maps are presented here as an interactive, multilayer portable document file (PDF), rather than as traditional pre-formatted map-sheet PDFs. The various data and base map elements are placed on separate layers, allowing the user to combine elements interactively to create map views in a dynamic fashion not possible with traditional map sheets. For example, fault lines, traditionally part of the geologic map sheet, can be overlain on the aeromagnetic data to examine the role of the faults as boundaries of bodies with differing magnetization. A layered PDF also allows the user to select simplified views by excluding some of the elements of a traditional map sheet, such as focusing on magnetization boundaries by omitting magnetic field contours. In addition, a layered PDF allows the user to select either a traditional topographic map base, a topographic shaded-relief base, or even no base at all.

To access the layers, open the PDF with Adobe Acrobat Reader or Acrobat. Layers may be viewed separately or in combination using the layers panel in the Acrobat navigation pane (vertical bar on the left side of the window). Click on the "Layers" icon to display available layers; turn layers off and on by clicking on the box to the left of the layer name. Map sheets with a traditional appearance are readily compiled by choosing the associated data layers or by choosing the desired map under "Bookmarks" icon in the navigation pane.

Filtering and Magnetization Boundaries

The dataset that resulted from merging the Burney (Langenheim, 2021) and Alturas (Langenheim, 2022) surveys was filtered to enhance different wavelength characteristics of the anomalies because wavelength can be a proxy for depth to the top of the anomaly source. Shorter wavelength anomalies are caused by shallow sources whereas longer wavelength anomalies are often caused by deeper sources. Note, however, because of the nature of potential field data like those discussed here, shallow sources can also produce long wavelength anomalies. This is especially pertinent for a thin magnetic sheet, a geometry expected for a lava flow.

First, these data were processed to account for the inclination and declination (65° and 15°, respectively) of the Earth's magnetic field in this region and to shift the anomalies over their causative sources. This operation is referred to as reduction to the pole and transforms the magnetic anomaly to that which would be measured at the magnetic north pole where the Earth's magnetic field is directed vertically down. A matched filter (Phillips, 2001) was then applied to the reduced-to-pole anomalies of the study area to separate the data into different wavelength components that can be related to depth. This is achieved by modeling the observed anomalies as a sum of anomalies from distinct equivalent source layers (fictional layers below the observation surface where the distribution of magnetization produces the observed magnetic field) at increasing depths. The matched-filter produced dipole-equivalent source layers at depths of 0.85 km (shallow), 3.28 km (medium), and 16.41 km (deep). Comparison of these fields (fig. 6) with the geology indicates that the shallow and medium layers generally reflect anomalies caused by Neogene volcanic rocks, whereas the deepest layer may be sensitive to sources in the underlying basement. As mentioned above, the actual source depths may be shallower, given that broader wavelength anomalies can be fit by both shallow and deep sources. This certainly applies to the deepest layer, given high heat flow and estimates of the depth to the Curie isotherm (approximately 580 °C) of about 16 km in this region (Bouligand and others, 2009). We also applied this method to a smaller area centered on Medicine Lake volcano, which produced equivalent source layers at depths of 0.8, 1.9, 4.18, and 9.75 km. A comparison of the magnetic fields from the deepest source layers shows small differences at these longer wavelengths (fig. 7), indicating that the depth values should be used with caution. Nonetheless, the pattern of magnetic highs and lows is consistent for the two deep long-wavelength fields (fig. 7).

To help delineate structural trends and gradients expressed in the magnetic fields, a computer algorithm was used to locate the maximum horizontal gradient (Cordell and Grauch, 1985; Blakely and Simpson, 1986). Faults beneath valley areas or thin basalt flows can be mapped using horizontal gradients in the magnetic fields, particularly where Quaternary and Tertiary volcanic rocks are offset by faults. Magnetization boundaries were calculated on filtered versions of the magnetic field as previously described. The magnetic fields were mathematically transformed into magnetic potential anomalies (Baranov, 1957); this procedure effectively converts the magnetic field to the equivalent "gravity" field that would be produced if all magnetic material were replaced by proportionately dense material. The horizontal gradient of the magnetic potential field was then calculated everywhere by numerical differentiation. The locations of the locally steepest horizontal gradient were determined by numerically searching for maxima in the horizontal gradient grid (Blakely and Simpson, 1986). Gradient maxima are present approximately over steeply dipping contacts that separate rocks of contrasting magnetizations. For moderate to steep dips (45˚ to vertical), the horizontal displacement of a gradient maximum from the top edge of an offset horizontal layer is always less than or equal to the depth to the top of the source (Grauch and Cordell, 1987). Boundaries were calculated from the match-filtered magnetic potential fields; those calculated from the shallow source field should reflect edges of magnetic sources near the ground surface (magnetic map and shallow magnetic map layer of map sheet 1).

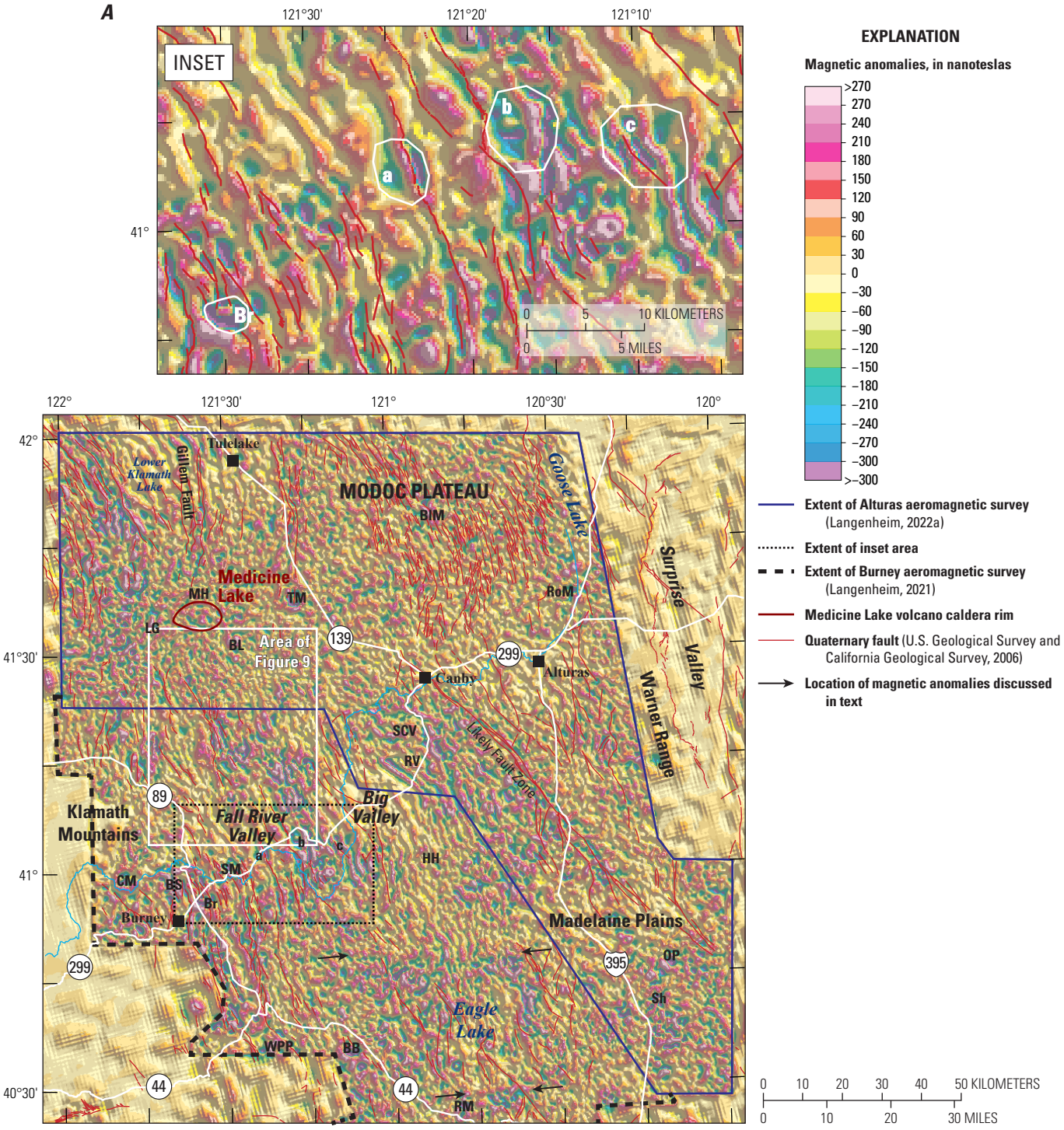

Figure 6 (pages 9–11). Colored shaded-relief-aeromagnetic map of northeastern California, filtered to enhance sources at various depths (nT, nanotesla[s]). All fields have been reduced to pole, which centers the anomalies over their sources by correcting for the inclination of the Earth's magnetic field. *A*, Match-filtered magnetic field with an equivalent source depth of 0.85 kilometer (km; shallow source). *B*, Match-filtered magnetic field with an equivalent source depth of 3.28 km (medium-depth source). *C*, Match-filtered magnetic field with an equivalent source depth of 16.4 km (deep source). Arrows point to linear anomalies that are not disrupted by strike-slip offset and a, b, and c refer to locations of semicircular magnetic anomalies discussed in Langenheim (2021). Geographic abbreviations: BB, Bogard Buttes; BL, Black Mountain, BIM, Blue Mountain, Br, Brush Mountain; BS, Burney Spring Mountain; CM, Chalk Mountain; HH, Hayden Hill; LG, Little Glass Mountain; MH, Mount Hoffman; OP, Observation Peak; RM, Roop Mountain; RoM, Round Mountain; RV, Round Valley; SCV, Stone Coal Valley; Sh, Shinn Mountain; SM, Saddle Mountain; TM, Timber Mountain; WPP, West Prospect Peak.

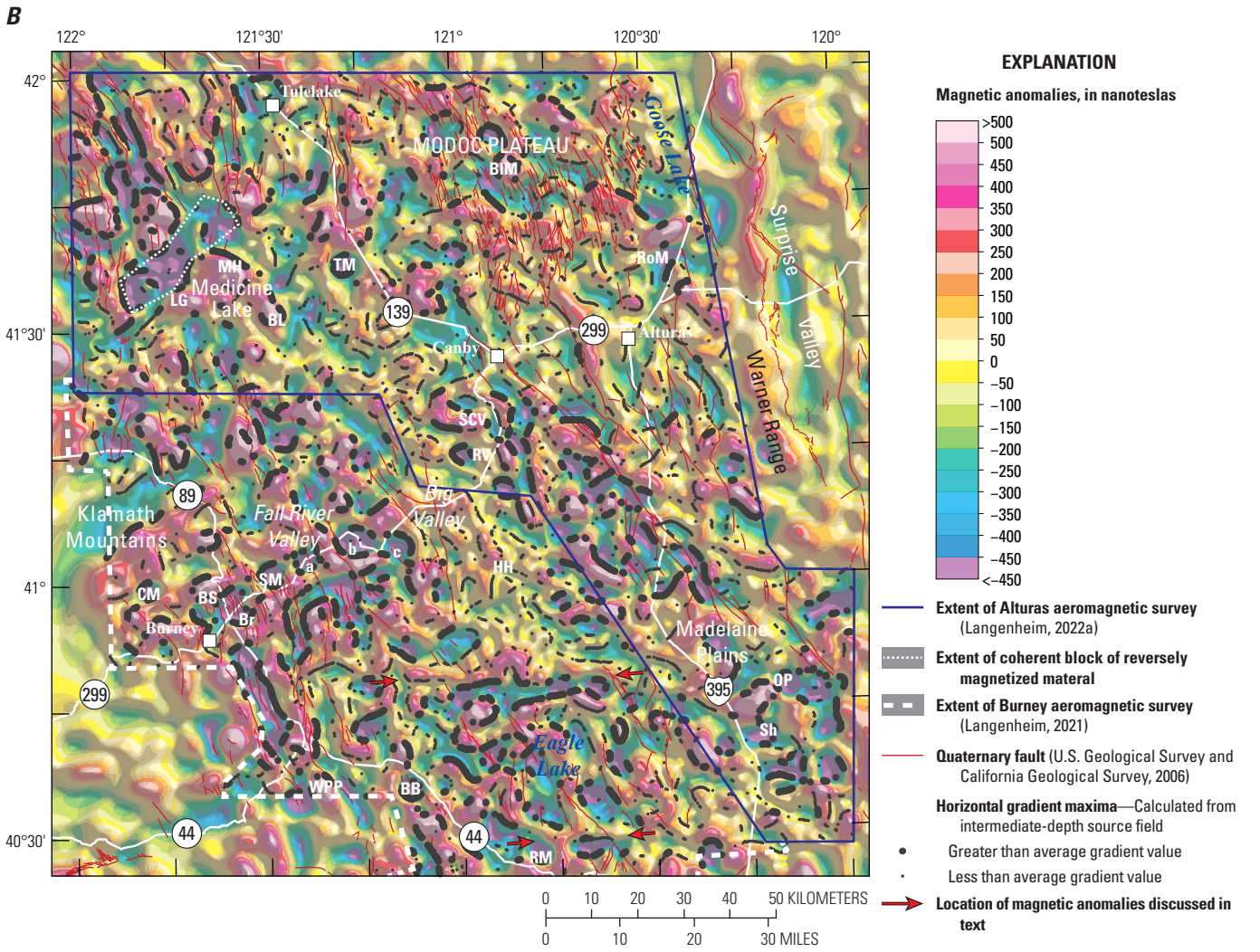

Figure 6 (pages 9–11). *Continued*

Results

Magnetic anomalies are generally caused by magnetite-bearing rocks, which are often igneous. Sedimentary rocks generally are not magnetic enough to produce measurable aeromagnetic anomalies. One first-order observation of the aeromagnetic dataset is that a relatively smooth magnetic field coincides with areas of sedimentary cover, such as Fall River Valley, Big Valley, Warm Springs Valley (between the town of Canby and the city of Alturas), Lower Klamath Lake and Tule Lake, as well as to some extent, Madeline Plains and Goose Lake (figs. 2, 3, 5*B*). Big and Fall River Valleys coincide with gravity lows (fig. 8) that have amplitudes of 20 milligals (mGal; Langenheim and others, 2016), indicating that these areas are underlain by thick sedimentary fill. Gravity lows of similar or greater amplitude underlie Tule and Lower Klamath Lakes (fig. 8; Braunsten, 2009). This is consistent with the attenuation of the magnetic anomalies in these areas because the magnetic source rocks are concealed by thick, nonmagnetic sedimentary fill. Another small gravity low beneath Round Valley (RV; northeast of Big Valley) also coincides with attenuated magnetic anomalies, consistent with a 10–12 mGal low constrained by a single profile of measurements along Highway 299 (figure 8; Chapman and Bishop, 1968). A gravity low of about 10 mGal coincides with part of Madeline Plains, although the measurements are widely spaced, thus, the amplitude and areal extent of the gravity anomaly are poorly constrained.

High-amplitude magnetic anomalies in the survey area are typically associated with volcanic rocks either exposed or in the shallow subsurface. In general, Quaternary volcanic rocks tend to be associated with short wavelength anomalies, for example, on the Modoc Plateau in the northeastern part of the study area and over the Medicine Lake highlands (fig. 6*A*). In contrast, Miocene and Pliocene volcanic rocks are generally associated with longer wavelength features that also have a longer mapped length, such as the volcanic rocks in the Big Valley Mountains to the northeast of Fall River Valley and those exposed in the area between Big Valley and the Likely Fault Zone (fig. 6*A*). Much of the area is characterized by short-wavelength, narrow, north-northwest-trending magnetic anomalies that are present over extensive areas of volcanic rocks, particularly southwest of the Likely Fault Zone (figs. 5*B*, 6*A*). These anomalies parallel the structural and topographic grain where faults associated with the northern end

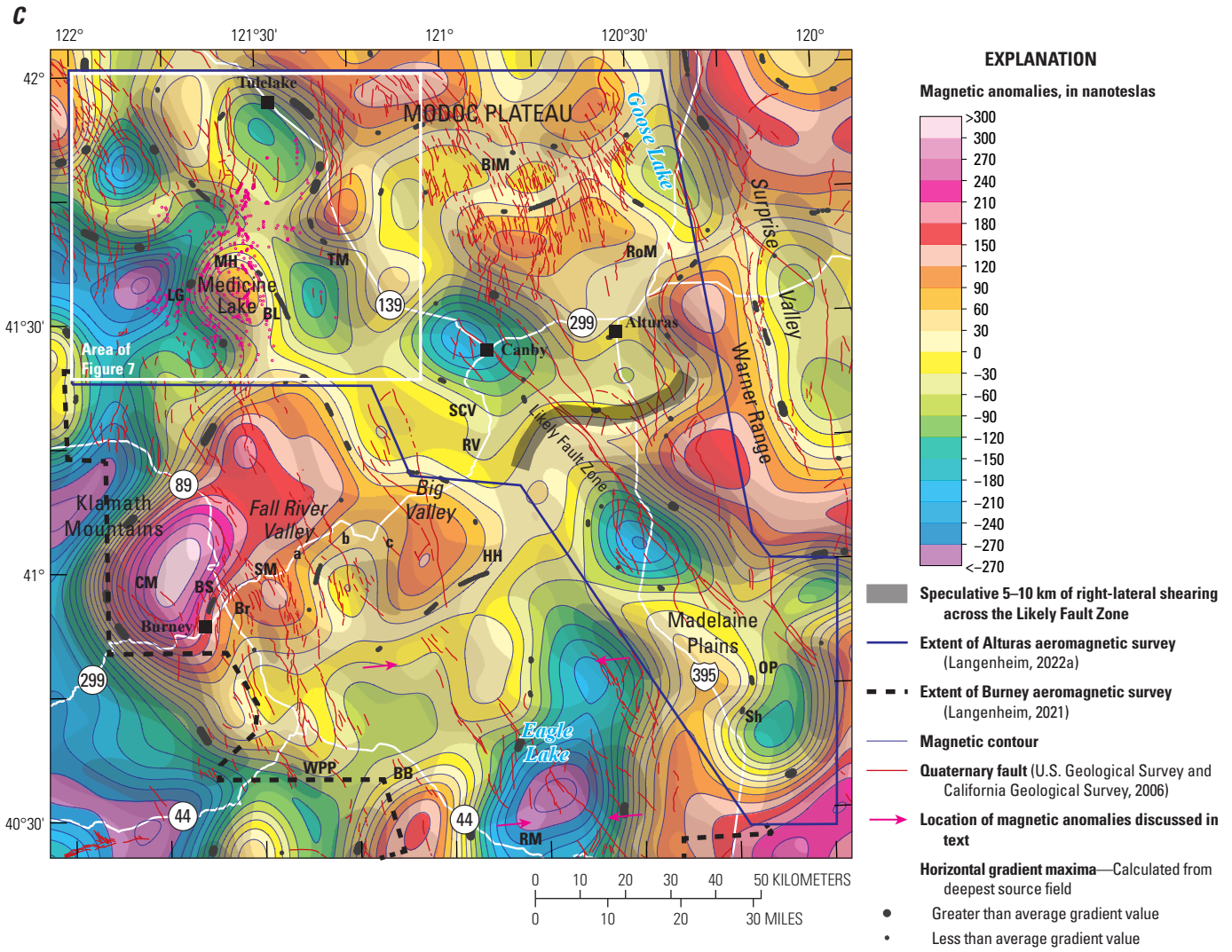

Figure 6 (pages 9–11). *Continued*

of the Walker Lane tectonic province offset volcanic rocks along north- and northwest-trending structures (Faulds and others, 2005; Waldien and others, 2019). The Modoc Plateau has a less pronounced magnetic grain (anomaly orientation and width; figs. 5*B*, 6*A*), likely because the numerous faults do not substantially offset the predominantly flat surface of the plateau (Hannah, 1977; U.S. Geological Survey and California Geological Survey, 2006). The subtle magnetic expression of the faults in this area confirms little cumulative vertical offset.

The Likely Fault Zone (figs. 3, 5*B*) is well expressed topographically and is inferred to have strike-slip offset, given its northwest orientation in the current stress field and right-laterally offset drainages in resistant bedrock (Sawyer and Bryant, 1995), yet no piercing points have been identified to ascertain the cumulative amount of offset since Miocene time. It also exhibits northeast-side down displacement and marks the boundary between few north-south or northeast-striking faults to the northeast of the structure versus abundant northwest-striking faults to the southwest (fig. 2; Grose, Egger, and O'Neil, 2016). The fault does coincide with magnetic gradients, which is expected given its topographic expression. A band of west-northwest-striking magnetic highs crosses the fault at an oblique angle and may be slightly offset along individual strands. The high in the filtered anomaly field to enhance deep sources (fig. 6*C*) may be sheared across the fault zone by about 5–10 km (speculatively). If so, the lack of absence of scarps on late Quaternary deposits and moderately to poorly defined scarps on resistant volcanic bedrock (fig. 3) argues that most of this slip is older than Quaternary. The magnetic expression of the fault suggests that it may change strike to a more northerly trend at its northwest mapped end (fig. 6*B)*.

Northwest-striking structures parallel to Likely Fault Zone were inferred by Duffield and Fournier (1974) by linking northwest-striking faults near the California-Oregon State line, assorted cinder cones, and shield volcanoes in the eastern half of the Modoc Plateau. Structures of this orientation do not appear to be supported by the magnetic data (fig. 6*A*); instead, the magnetic data show subtle east-northeast (fig. 6*A, C*) or east-west (fig. 6*B*) magnetic anomalies that are nearly perpendicular to the trend of distributed normal faulting on the Modoc Plateau. An inferred tear in the subducting Farallon Plate during the Eocene to Miocene projects east-northeast across the plateau (Colgan and others, 2011; fig. 1). Magnetotelluric and gravity anomalies also share

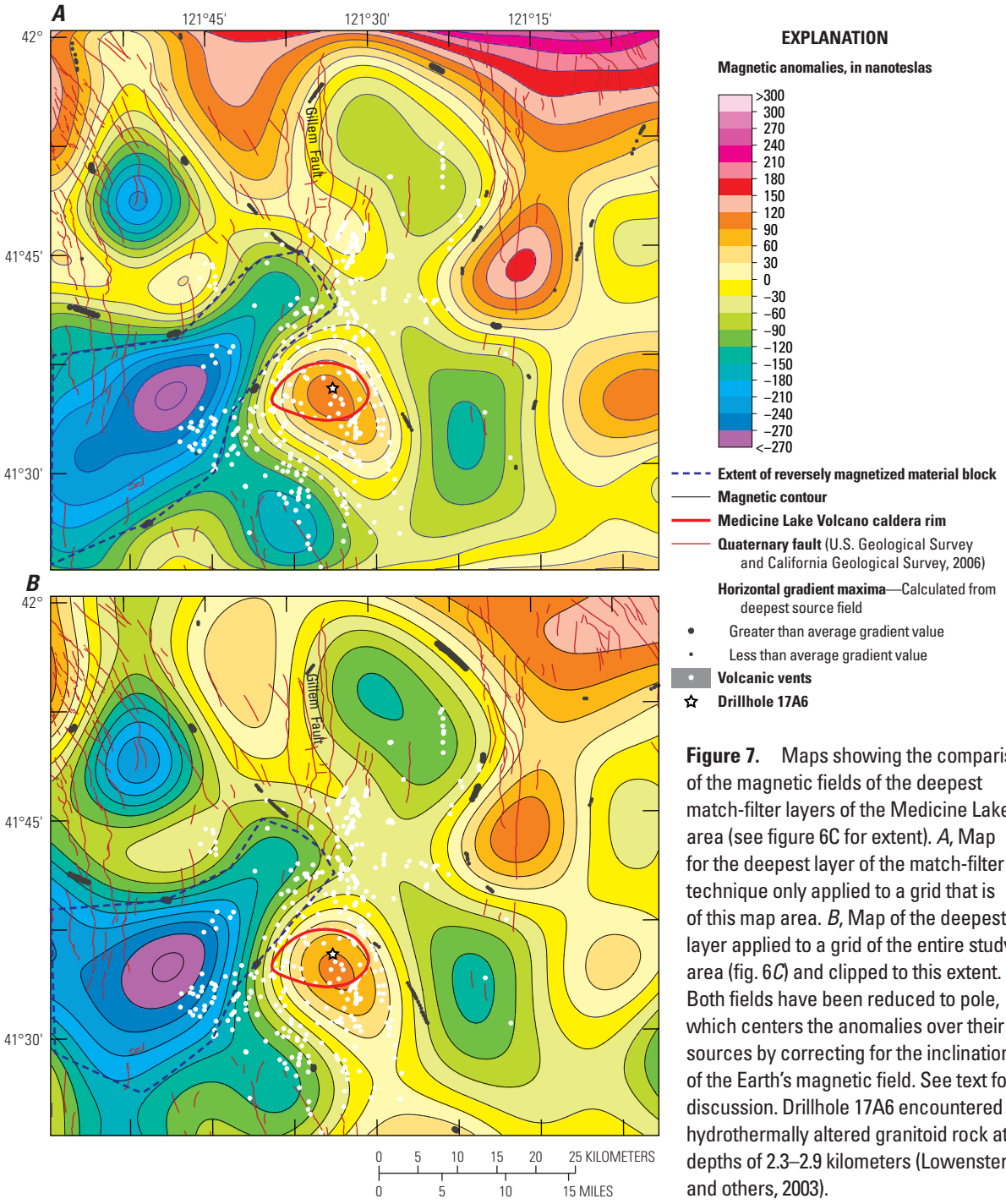

Figure 7. Maps showing the comparison of the magnetic fields of the deepest match-filter layers of the Medicine Lake area (see figure 6C for extent). *A*, Map for the deepest layer of the match-filter technique only applied to a grid that is of this map area. *B*, Map of the deepest layer applied to a grid of the entire study area (fig. 6*C*) and clipped to this extent. Both fields have been reduced to pole, which centers the anomalies over their sources by correcting for the inclination of the Earth's magnetic field. See text for discussion. Drillhole 17A6 encountered hydrothermally altered granitoid rock at depths of 2.3–2.9 kilometers (Lowenstern and others, 2003).

similar trends across the broader study region and may reflect deeper basement and mantle structure (fig. 1; Bedrosian and Feucht, 2014; Blakely and others, 1997).

The new aeromagnetic data also reveal two long (20 and 45 km), linear, east-west-trending magnetic anomalies that do not coincide with topographic and geologic features and that are not disrupted by strike-slip offset (features marked by pairs of arrows on figs. 5*B* and 6*A*). The southernmost of these is not evident in the older data (fig. 5*A*). These anomalies cross several mapped Quaternary faults without showing substantial (>2 km) apparent right-lateral offset. A possible exception is the fault zone that cuts across the western part of the Madeline Plains, where a magnetic high appears to be offset by about 5 km (just east of the 45-km-long linear east-west magnetic anomaly; figs. 5*B*, 6*A*, and 6*B*). The presence of these continuous anomalies places limits on the amount of dextral offset that may be ascribed to faults in this northern part of the Walker Lane tectonic province.

The western third of the combined survey area includes the south end of the Cascades volcanic arc, including the Lassen Peak segment (Clynne and Muffler, 2017) near the southwest corner of the surveyed area and the Medicine Lake volcano (Donnelly-Nolan, 2010; Donnelly-Nolan and Grove, 2017) in the northwest. The youngest arc-affiliated rocks are built on a platform of coalescing andesitic volcanoes and thin but widespread basaltic

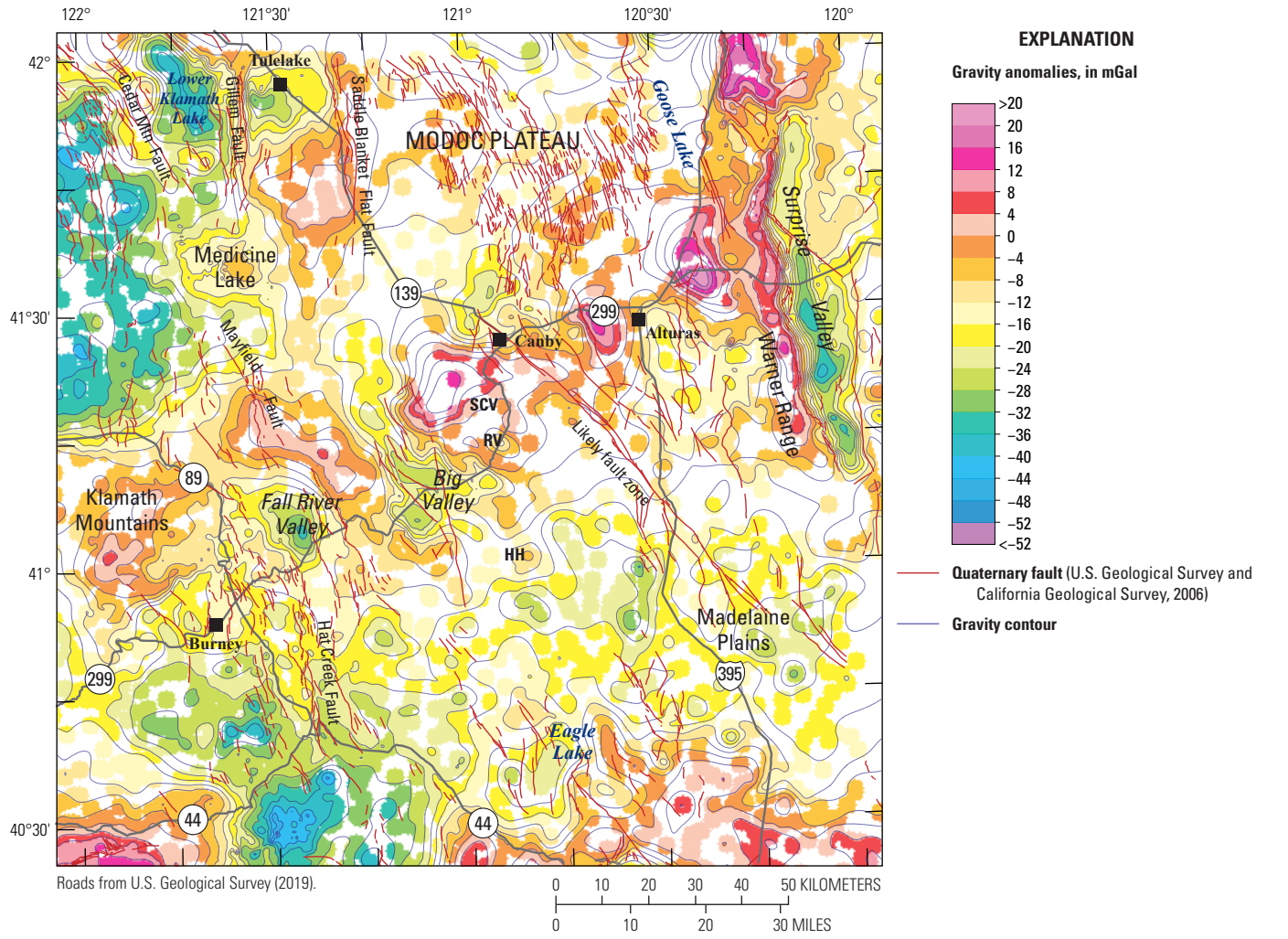

Figure 8. Isostatic gravity map of northeastern California. Color background extends along a 2-kilometer radius from each gravity measurement. Data from Chapman and Bishop (1968), Brauntsen (2009), Pan-American Center for Earth and Environmental Studies (2010), and Langenheim and others (2016). Geographic abbreviations: HH, Hayden Hill; RV, Round Valley; SCV, Stone Coal Valley. Mtn, Mountain.

flows (Clynne and Muffler, 2017). The coalescing volcanoes are calc-alkaline in composition, dominated by basaltic andesite and andesites, and range in size and morphology from scoria cones to steep-sided lava cones to broad shield volcanoes (Clynne and Muffler, 2017). Magnetic anomalies associated with these volcanic edifices interrupt the dominant magnetic grain, appearing as complex semicircular features on the map showing magnetic data filtered to emphasize shallow sources (fig. 6*A*) and as more coherent circular features on the map showing magnetic data filtered to emphasize intermediate-depth sources (fig 6*B*).

As pointed out previously (Langenheim and others, 2016; Langenheim, 2021) several of these prominent semicircular magnetic highs and lows are ascribed to young lava cones or shield volcanoes, such as Bogard Buttes, West Prospect Peak, Brush Mountain, Burney Springs Mountain, Chalk Mountain, and Saddle Mountain (fig. 5*B*); the magnetic polarity of the rocks that form these volcanoes determines whether the edifice is marked by a positive or negative anomaly and may help constrain the age of the feature (Langenheim and others, 2016). For example, the large magnetic low coincident with Timber Mountain indicates that the true age of the older basaltic andesite of Timber Mountain (map unit "omt" of Donnelly-Nolan, 2010) is within the lower range of uncertainty of its younger date (1.80 ± 0.06 Ma; Donnelly-Nolan and Lanphere, 2005) and erupted during chron C1r.3r (Ogg, 2020) whereas a semicircular low at Roop Mountain (figs. 1, 5*B*) is consistent with a nearby age of 3.9 ± 0.2 millions of years ago (Ma) (Grose, Saucedo, and Wagner, 2014b) during chron C2Ar (Ogg, 2020). The magnetic high associated with Blue Mountain suggests that the true age of the volcano is not represented by its mean K-Ar age of 5.4 Ma, which lies within reversed chron C3r (Ogg, 2020). Negative anomalies coincide with Shinn Mountain and Observation Peak, consistent with their age dates of 12.15–12.09 Ma and 4.02 ± 0.11 Ma, respectively (Grose, Saucedo, and Wagner, 2014a). However, a prominent volcano does not always correspond to a simple magnetic high or low, which may be indicative of complexity within the volcanic stratigraphy that makes up the volcano. For example, a small circular magnetic high suggests that a vent of normal polarity is either unmapped or concealed at shallow depth about 1.2 km northeast of Observation Peak (figs. 5*B*, 6*A*).

Thick sections of silicic tuffaceous rocks have been interpreted to have accumulated in caldera settings at Hayden Hill, 60 km south-southwest of the City of Alturas, Calif. (Hazlett, 1984; Finn, 1987) and in Stone Coal Valley, 48 km west-southwest of the City of Alturas, Calif. (Bowens, 1998; Bowens and Grose, 2001; Grose, Egger, and O'Neil, 2016). At Hayden Hill, the aeromagnetic data do not appear to support a caldera interpretation. In Stone Coal Valley, the aeromagnetic data show an oblong magnetic low surrounded by magnetic highs (fig. 5*B*); neither a definitive ring fracture nor evidence for an intracaldera facies of a tuff are identified by geologic mapping (Bowens, 1998; Grose, Egger, and O'Neil, 2016). The section of silicic tuffaceous rocks in Stone Coal Valley may have their source at local rhyolitic volcanic centers, rather than from a caldera collapse. Existing gravity data in Stone Coal Valley, although sparse, indicate a gravity high in this area (fig. 8; Chapman and Bishop, 1968), opposite of what is predicted for a thick accumulation of tuffaceous rocks. Instead, the gravity high was attributed by Bowens and Grose (2001) to intrusive rocks underlying the volcanic sequence, similar to the interpretation of rocks beneath Medicine Lake volcano. Another explanation for the gravity high invokes near-surface basement rocks (Chapman and Bishop, 1968).

The largest volcanic edifice in the study area, Medicine Lake volcano, coincides with a complex magnetic high, consistent with its having been constructed during the past 500 thousand years during a normal chron (Donnelly-Nolan, 2010). Some relative magnetic lows approximately coincide with topographic lows, possibly owing to terrain effects but other superposed lows and highs may indicate variations in magnetization. The magnetic field filtered to enhance intermediate-depth sources indicates three main magnetic sources centered roughly on Black Mountain, Mount Hoffman, and Little Glass Mountain (fig. 6*B*). At longer wavelengths (figs. 6*C* and 7), these highs coalesce to a single positive anomaly that may reflect an intrusive body underpinning the edifice as interpreted from analysis of gravity (Finn and Williams, 1982) as well as seismic (Zucca and others, 1986, Fuis and others, 1987, Chiarabba and others, 1995) and magnetotelluric data (Stanley and others, 1990), although the shape of the body derived from gravity shown in figure 8 is more elongate in an east-west direction than the shape of the anomaly in figure 7. Two drill holes at depths of 2.3–2.9 km encountered hydrothermally altered granodiorite and granitoid; Lowenstern and others (2003) dated the granodiorite at 319 ± 8 kilo-annum (ka) and suggested that this body is the source of the geophysical anomalies. If so, the gravity, seismic tomographic, and magnetotelluric models could be refined such that the modeled top of the body is about 1 km deeper to fit the drillhole constraints. Northwest of the Medicine Lake magnetic highs, negative anomalies form a 10-km-wide, northeast-striking belt (figs. 6*B*, 7). In places terrain consists of some older units whose ages are within reversed magnetochrons; the magnetic data indicate a coherent block of reversely magnetized material that trends northeast to the south end of the Gillem Fault (figs. 5*B*, 6*B,* 7). This block roughly coincides with a "kink" in the pattern of faulting, where north-northwest-striking faults entering the volcano turn to the north-northeast, and then back to the north and northwest (Donnelly-Nolan and others, 2008). Within and along the southern margin of the block, more vents appear to be aligned in a northeast direction (fig. 7; also compare geology/vents layer with shallow, intermediate-source, and deep magnetic field layers in map sheet 1), suggesting that the block may reflect a deep-seated structural control.

Another example of insights of volcanic stratigraphy from the magnetic data is the magnetic low associated with Brushy Mountain (Br in figure 5*B)*. Filtered data reveal a small magnetic high within the low (inset in figure 6*A;* see also map sheet 1). This small magnetic high, which was not discernible in the earlier, lower resolution data (Langenheim, 2021*)*, supports the interpretation from paleomagnetic data that the bulk of the volcano is reversed polarity, except for the top of the edifice, which consists of normal-polarity flows.

The detailed data also reveal that some of these semicircular anomalies are, in fact, more complicated; in this case, they are bisected by narrow, linear magnetic highs (see, for example, anomalies a, b, and c in figures 5*B*, 6*A*; Langenheim and others, 2016). The narrow anomaly that bisects the negative anomaly a coincides with a mapped Quaternary fault. A similar narrow anomaly cuts across anomaly b (figure 6*A*). These narrow anomalies are most probably fault related and may be related to a short, mapped Quaternary fault a few kilometers to the south. Anomaly c appears less semicircular in the detailed data and is bisected by two narrow magnetic highs (fig. 6*A)*. One of the highs is nearly coincident with a short, mapped fault and extends about 5 km to the north and south of the fault. However, the southward continuation coincides with a prominent topographic ridge that may not reflect Quaternary fault offset.

Linear, narrow magnetic anomalies are often associated with mapped Quaternary faults (fig. 5*B*), most notably along the Hat Creek Fault, but also along the Gillem, Mayfield, Saddle Blanket Flat and Cedar Mountain Faults. Similar linear magnetic highs across Fall River Valley can be interpreted as faults concealed beneath the young sedimentary deposits; some of these highs extend north towards Medicine Lake volcano and may provide pathways for groundwater flow from the highlands to the springs in Fall River Valley. Similarly, linear magnetic anomalies support extending mapped faults along the southern margin beneath Tule and upper Klamath Lakes.

The importance of magnetic terrain is highlighted by the comparison of the magnetic field filtered to enhance shallow sources (fig. 9*A*) and the magnetic field predicted by magnetic terrain of normal polarity (fig. 9*B*) for the area south of Medicine Lake volcano. The predicted magnetic field was created assuming that the terrain has a magnetization of 0.01 electromagnetic unit per cubic centimeter (10 ampere per meter), a flat bottom, and an average thickness of ~160 m using the technique described in Blakely (1981). In particular, in areas covered by extensive basalt flows mapped as a single unit by its characteristic paleomagnetic directions (for example, basalts of Giant Crater and Yellowjacket Butte, both of normal polarity), some of the subtle positive anomalies over parts of the flows can be attributed to topographic effects. In other places, negative anomalies highlight sources that are concealed beneath the flows, such as beneath the basalt of Yellowjacket Butte (Donnelly-Nolan, 2010; r in figure 9). The comparison also indicates where basalt of Giant Crater (Donnelly-Nolan, 2010; or other underlying normal-polarity flows) thickens against the Mayfield Fault Zone (t in figure 9). Although multiple strands of the Mayfield Fault Zone are mapped, the ones with the most cumulative offset are likely those that coincide with magnetic boundaries. Outside of the young basalt flows, other areas show a magnetic high predicted where a magnetic low is observed, indicating that

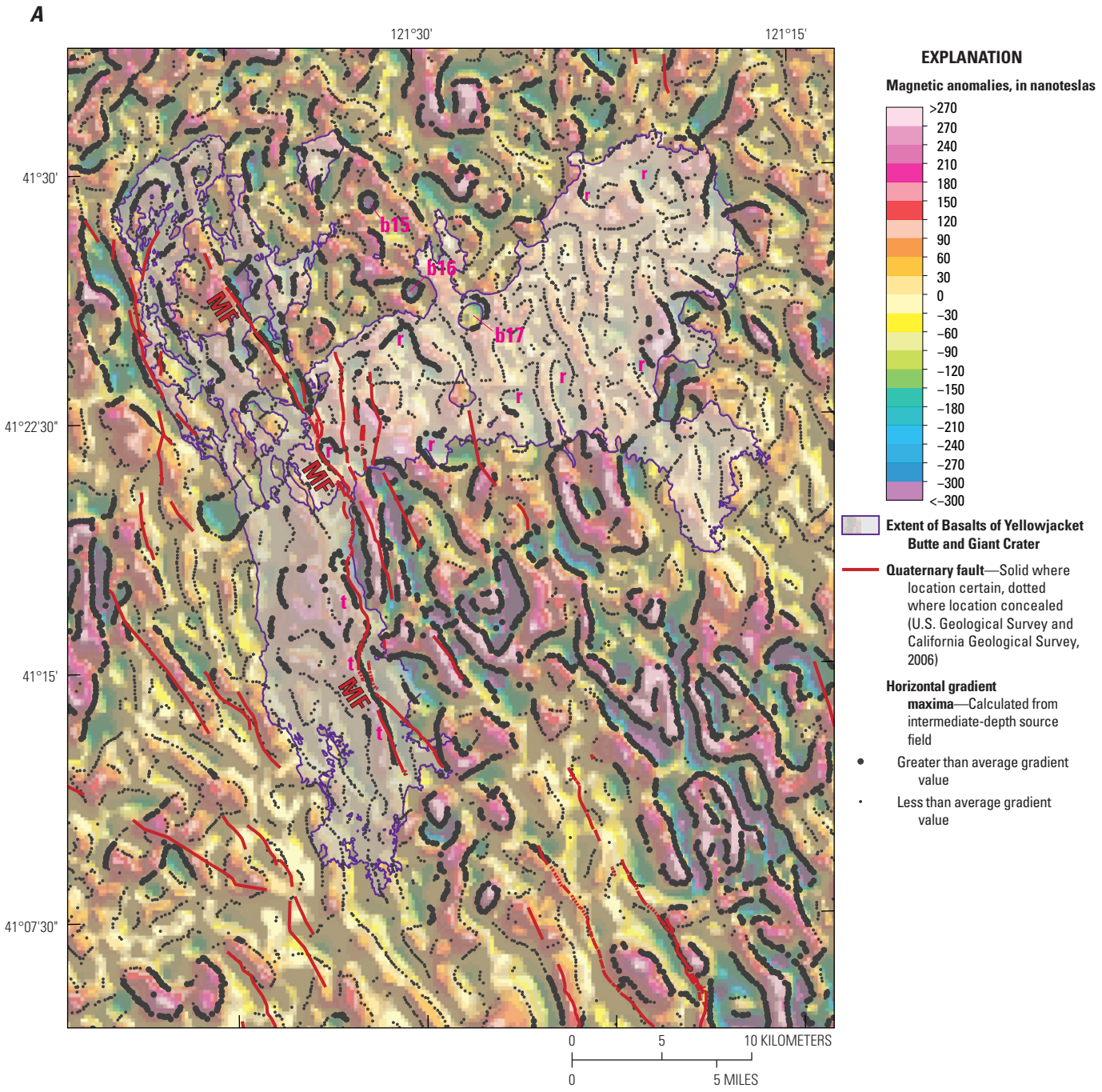

Figure 9 (pages 12–13). Filtered and predicted magnetic anomaly maps of area outlined in figure 6*A*. *A*, magnetic anomaly map filtered for shallow sources. *B*, predicted magnetic anomalies from magnetic terrain. Both fields are reduced to pole, which centers the anomalies over their sources by correcting for the inclination of Earth's magnetic field. White and gray transparent polygons denote extent of the basalts of Yellowjacket Butte and Giant Crater, respectively (Donnelly-Nolan, 2010). "b15-b17" are basalt cinder cones mapped by Donnelly-Nolan (2010). "r" indicates negative anomalies observed within the normally polarized basalt of Yellowjacket Butte. "t" indicates magnetic highs interpreted to be thicker Giant Crater basalt and (or) underlying normally polarized units. Note for part B, the east-trending step of higher values is an artifact resulting from the boundary between the Burney and Alturas surveys flown at different heights. MF, Mayfield fault zone.

the topography is composed of material of reversed polarity. For example, cinder cones labeled b15–b17 coincide with circular negative anomalies in the observed data but are positive anomalies in the predicted field. This relationship indicates these cones were erupted before the Brunhes normal chron (>773 ka; Ogg, 2020) and suggests that these cones may be somewhat older than the inferred age of middle Pleistocene (Donnelly-Nolan, 2010).

Smoother magnetic anomalies (fig. 5*A)* also coincide with extensive outcrops of Paleozoic and Mesozoic sedimentary rocks in the eastern Klamath Mountains (fig. 3), although the greater

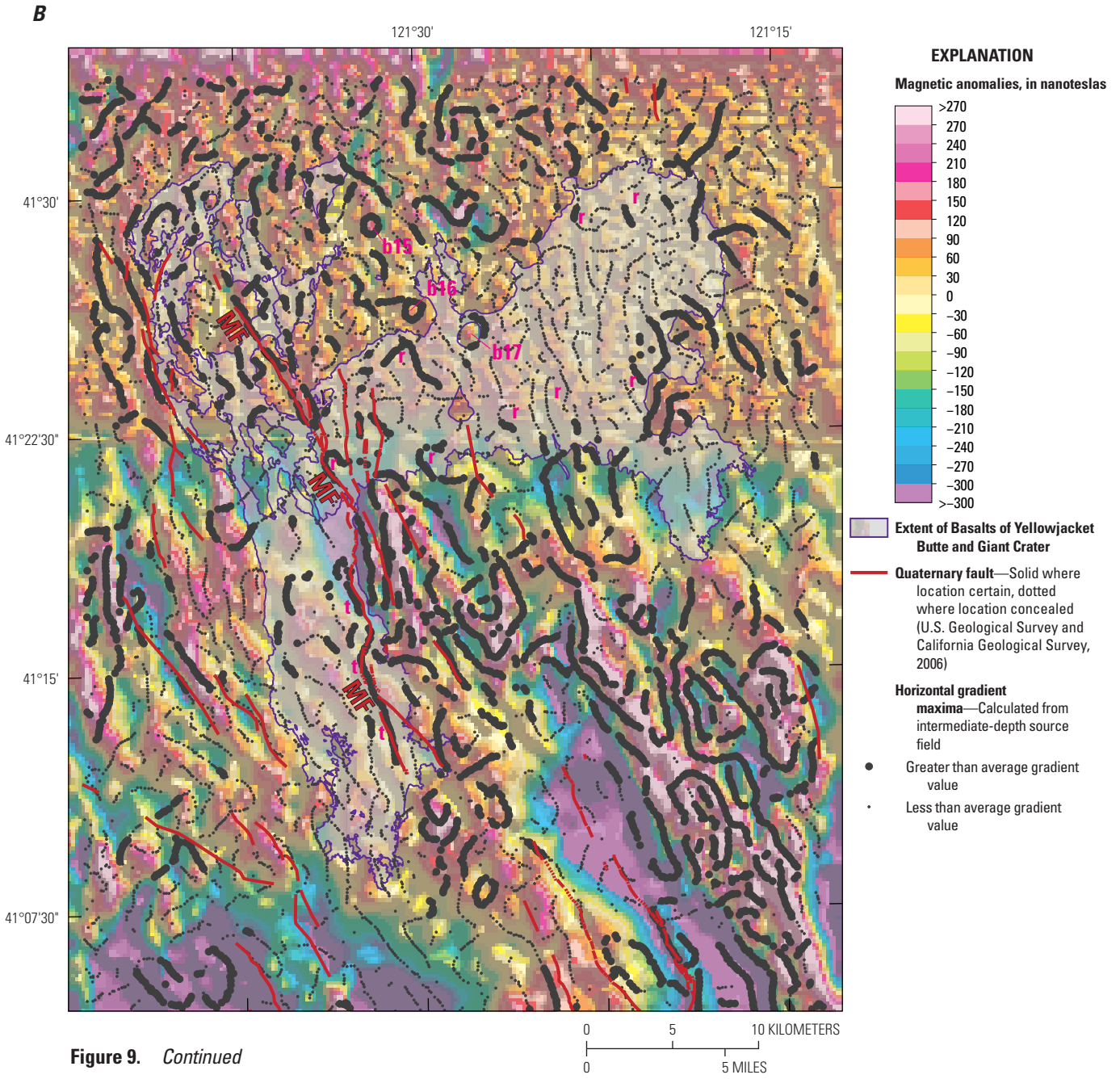

Figure 9. *Continued*

height of the survey above this area (fig. 4) also contributes to the smoothing and broadening of magnetic anomalies. The Paleozoic and Mesozoic sedimentary rocks coincide with low magnetic values; however, a major northeast-striking magnetic high seen best in the magnetic field filtered for deep sources (near CM in figure 6*C*) underlies part of the eastern Klamath Mountains and is attributed to mafic pre-Cenozoic basement (Langenheim and others, 2016). The outcrops of Cretaceous granitic rocks south of Eagle Lake coincide with a magnetic high, consistent with measurements elsewhere in the northern Sierra Nevada that indicate these rocks are moderately magnetic (Langenheim and others, 2019). Relatively low magnetic values coincide with rocks mapped as pre-Cretaceous schist, gneiss, and amphibolite along the northern margin of the Cretaceous granitic rocks (Grose, Saucedo, and Wagner, 2014a). These outcrops lie within a north-striking magnetic low in the filtered magnetic data (fig. 6*C*), indicating that the Cretaceous granitic rocks may not make up a substantial crustal volume there or that its magnetic signal is swamped by strongly magnetic, reversely magnetized volcanic rocks, such as those comprising Roop Mountain.

In summary, the aeromagnetic maps combined with the geologic map, provide insight into the continuity of faults that offset volcanic rocks, such as those in Fall River Valley and the Tule and Lower Klamath Lake areas. These data also indicate the magnetic polarity of volcanoes and cinder cones that can better constrain the age of those features. Magnetic anomalies constrain the amount of right-lateral offset on faults, such as the Likely Fault Zone and faults west of the Madeline Plains and east of Roop Mountain. Filtered magnetic anomalies reveal a northeast-striking, fault-bounded block of predominantly reversed material that may influence tectonism at Medicine Lake volcano.

DESCRIPTION OF MAP UNITS

QUATERNARY AND RECENT VOLCANIC ROCKS

QHv **Quaternary and Holocene volcanic rocks (Holocene to Quaternary)**—In eastern part of map area, local recent (Holocene) basalt and mafic andesite flows with minor pyroclastic deposits; in part Pleistocene. In northwestern part of map area, basalt and mafic andesite flows associated with the Medicine Lake volcano complex, including basaltic vent facies and flows, a single dacitic ash-flow tuff, and localized dacite-to-rhyolite lava flows (Donnelly-Nolan, 2010). In southwestern part of map area, a heterogeneous assemblage of small to medium sized andesitic stratovolcanoes consisting predominantly of basalt, basaltic andesite, and andesite; dacite domes surrounded by andesite flows, and small-volume but widespread low-potassium olivine tholeiite basalt lava flows that fill topographic lows such as Hat Creek graben (Muffler and others, 1994; Clynne and Muffler, 2010). Two Quaternary basaltic flows are mapped separately, as:

QHvg **Basalt of Giant Crater of Donnelly-Nolan (2010) (late Pleistocene)**—Chemically variable basaltic lava field, extending 45 km south from source vents on south flank of Medicine Lake Volcano; includes both ʻaʻā and pāhoehoe lavas. Calibrated age of 12,430 years before present (Donnelly-Nolan, 2010)

QHvh **Hat Creek Basalt (late Pleistocene)**—Tholeiitic olivine basalt lava-flow complex, consists of many flow units erupted from a 3 km-long fissure capped by spatter cones near southern extent of unit. Lava flowed north into and filled Hat Creek Graben for 20 km to the north. Reported $^{40}Ar/^{39}Ar$ age of 24 ± 6 ka (Turrin and others, 2007)

QUATERNARY SEDIMENT AND CENOZOIC SEDIMENTARY ROCKS

QTs **Quaternary deposits and Tertiary sedimentary rocks (Quaternary to Tertiary)**—Holocene and Pleistocene deposits include unconsolidated sand, gravel, and silt associated with modern fluvial systems, alluvial fans, and sand sheet deposits; local massive- to thin-bedded accumulations of silt, clay, and sand as unconsolidated, subhorizontal lacustrine deposits. North of Burney, Calif., in Pit River drainage, lacustrine deposits form thick accumulation of poorly to moderately consolidated diatomite (Clynne and Muffler, 2017). Late Miocene and Pliocene sedimentary rocks include the Alturas Formation, approximately 200–300 m of volcaniclastic, tuffaceous, and diatomaceous sedimentary rocks exposed in valleys in eastern third of map area (Collins, 1999), and thick sections of fine grained, bedded lapilli tuff and interbedded sandstone and conglomerate that underlie Fall River Valley and Big Valley near center of map area (Grose and others, 2016).

Temc **Montgomery Creek Formation (Eocene)**—Partly consolidated, thick-bedded arkosic sandstone, conglomerate, and shale; locally includes coal beds. Nonmarine and mostly fluviatile (Macdonald, 1966); 300–800 m thick. Rests unconformably on Late Cretaceous and older rocks west of map area.

CENOZOIC VOLCANIC ROCKS

Tvu **Tertiary volcanic rocks, undivided (Tertiary)**—In northeast part of map area, basalt flows of Devil's Garden form volcanic plateau west of Alturas, Calif. comprised of series of olivine basalt lava flows with local vents facies and cinder cones, basalts in part Pliocene and Miocene (McKee and others, 1983; Hart and others, 1984). Much of east-central and southeastern part of map area features coalescing field of deeply eroded Middle to Late Miocene dominantly andesitic shield and stratovolcanoes composed of basalt, basaltic-andesite, and andesitic lava flows and pyroclastic deposits (Grose, 2000; Grose, Saucedo, and Wagner, 2014a, b; Grose, Egger, and O'Neil 2016, 2017); up to 2–3 km thick. Tertiary volcanic rocks in center of map include series of basalt and andesite flows, dacite tuff, and volcaniclastic rocks; largely Miocene; source vents poorly defined (Bean, 1980; Grose, 2000).

MESOZOIC SEDIMENTARY ROCKS

Ŧru **Triassic rocks, undivided (Triassic)**—Includes Modin Formation and Brock Shale, undivided (Irwin, 1994; Fraticelli and others, 2012). Modin Formation consists of basal coarse pyroclastic and conglomerate beds, middle unit of tuffaceous limestone and sandstone, and upper thin-bedded argillite; total thickness approximately 1,675 m. Modin Formation appears to conformably overlie Brock Shale, a 120-m-thick interval of argillite and interbeds of tuff and tuffaceous sandstone

MESOZOIC IGNEOUS ROCKS

Kgr **Cretaceous granitic rocks (Cretaceous)**—Hornblende-biotite granodiorite, medium-grained, massive, mostly uniform but locally with aplitic, pegmatitic and seriate textures and elongate mafic xenoliths. Locally in sharp to gradational contact with roof pendants of schist, gneiss, and amphibolite that are massive to strongly foliated and likely derived from sedimentary and volcanic protoliths

References Cited

Baranov, V.I., 1957, A new method for interpretation of aeromagnetic maps—Pseudo-gravimetric anomalies: Geophysics, v. 22, p. 359–383.

Bean, S.M., 1980, Volcanotectonics and geothermal potential in the Big Jack Lake area, Lassen County, California: Golden, Colorado, Colorado School of Mines M.S. thesis, 103 p., 2 pl.

Bedrosian, P.A., and Feucht, D.W., 2014, Structure and tectonics of the northwestern United States from EarthScope USArray magnetotelluric data: Earth and Planetary Science Letters, v. 402, p. 275–289, https://doi.org/10.1016/j.epsl.2013.07.035.

Blakely, R.J., 1981, A program for rapidly computing the magnetic anomaly over digital topography: U.S. Geological Survey Open-File Report 81–298, 46 p.

Blakely, R.J., 1995, Potential theory in gravity and magnetic applications: Cambridge, England, Cambridge University Press, 441 p.

Blakely, R.J., Christiansen, R.L., Guffanti, M., Wells, R.E., Donnelly-Nolan, J.M., Muffler, L.J.P., Clynne, M.A., and Smith, J.G., 1997, Gravity anomalies, Quaternary vents, and Quaternary faults in the southern Cascade Range, Oregon and California—implications for arc and backarc evolution: Journal of Geophysical Research, v. 102, p. 22,513–22,527.

Blakely, R.J., and Simpson, R.W., 1986, Approximating edges of source bodies from magnetic or gravity anomalies: Geophysics, v. 51, p. 1494–1498.

Bouligand, C, Glen, J.M.G., and Blakely, R.J., 2009, Mapping Curie temperature depth in the western United States with a fractal model for crustal magnetization: Journal of Geophysical Research, v. 114, no. B11104, https://doi.org/10.1029/2009JB006494.

Bowens, T.E., 1998, Geology and mineral deposit reconnaissance in the Stone Coal Valley region, Modoc County, California: Golden, Colorado School of Mines, M.S. thesis, 145 p., 3 pls.

Bowens, T.E., and Grose, T.L., 2001, Probable mid-Miocene caldera in the Modoc Plateau, northeast California: 2001 American Geophysical Union Fall Meeting, abstract V52A-1047.

Braunsten, S.B., 2009, Subsurface structure of the Lower Klamath Lake and Tule Lake basins, California, investigated using gravity anomalies: M.S. thesis, Portland State University, 112 p.

Briggs, I.C., 1974, Machine contouring using minimum curvature: Geophysics, v. 39, p. 39–48.

California Geological Survey, 2019, Historic Earthquake Online Database: California Geological Survey website, accessed July 2, 2017, at https://maps.conservation.ca.gov/cgs/historicearthquakes/.

Chapman, R.H., and Bishop, C.C., 1968, Bouguer gravity map of California—Alturas sheet: California Division of Mines and Geology, scale 1:250,000, 3 p.

Chiarabba, C., Amato, A. and Evans, J.R., 1995, Variations on the NeHT high-resolution tomography method—A test of technique and results for Medicine Lake volcano, northern California: Journal of Geophysical Research, v. 100, no. B3, p. 4035–4052.

Clynne, M.A., and Muffler, L.J.P., 2010, Geologic map of Lassen Volcanic National Park and vicinity, California: U.S. Geological Survey Scientific Investigations Map 2899, 95 p., 3 sheets, https://doi.org/10.3133/sim2899.

Clynne, M.A., and Muffler, L.J.P., 2017, Geologic field-trip guide to the Lassen segment of the Cascades Arc, northern California: U.S. Geological Survey Scientific Investigations Report 2017–5022–K2, 65 p., accessed June 6, 2019, at https://doi.org/10.3133/sir20175022K2.

Colgan, J.P., Egger, A.E., John, D.A., Cousens, B., Fleck, R.J., and Henry, C.D., 2011, Oligocene and Miocene arc volcanism in northeastern California: Evidence for post-Eocene segmentation of the subducting Farallon plate: Geosphere, v. 7, p. 733–755, https://doi.org/10.1130/GES00650.1.

Collins, N.E., 1999, Stratigraphy and geochemistry of the Alturas Formation, Modoc Plateau, northeastern California: Humboldt State University, Arcata, M.S. Thesis.

Cordell, L., and Grauch, V.J.S., 1985, Mapping basement magnetization zones from aeromagnetic data in the San Juan Basin, New Mexico, *in* Hinze, W.J., ed., The utility of regional gravity and magnetic anomaly maps: Tulsa, Okla., Society of Exploration Geophysicists, p. 181–197.

Couch, R., and Gemperle, M., 1982, Aeromagnetic measurements in the Cascade Range and Modoc Plateau of northern California—Report on work done from June 1, 1980, to November 30, 1980: U.S. Geological Survey Open-File Report 82–932, 23 p.

Cumming, W., and Mackie, R., 2010, Resistivity imaging of geothermal resources using 1D, 2D, and 3D MT inversion and TDEM static shift correction illustrated by a Glass Mountain case history: Proceedings World Geothermal Congress, 25–29 April 2010, Bali, Indonesia, p. 1–10.

Davisson, M.L., and Rose, T.P., 2014, Recharge and flow in the Medicine Lake volcano—Fall River Springs groundwater basin, California: Environmental Forensics, v. 15, p. 66–77.

Donnelly-Nolan, J.M., 2010, Geologic map of Medicine Lake volcano, northern California: U.S. Geological Survey Scientific Investigations Map 2927, 2 sheets, scale 1:50.000, pamphlet 48 p., accessed May 15, 2019, at https://doi.org/10.3133/sim2927.

Donnelly-Nolan, J.M., and Grove, T.L., 2017, Geologic field-trip guide to Medicine Lake volcano, northern California, including Lava Beds National Monument: U.S. Geological Survey Scientific Investigations Report 2017–5022–K1, 53 p., https://doi.org/10.3133/sir20175022K1.

Donnelly-Nolan, J.M., and Lanphere, M.A., 2005, Argon dating at and near Medicine Lake volcano, California—Results and data: U.S. Geological Survey Open-File Report 2005-1416, 37 p.

Donnelly-Nolan, J.M., Grove, T.L., Lanphere, M.A., Champion, D.E., Ramsey, D.W., 2008, Eruptive history and tectonic setting of Medicine Lake volcano, a large rear-arc volcano in the southern Cascades: Journal of Volcanology and Geothermal Research, v. 177, p. 313–328.

du Bray, E.A., John, D.A., Putirka, Keith, and Cousens, B.L., 2009, Geochemical database for igneous rocks of the ancestral Cascades arc—Southern segment, California and Nevada: U.S. Geological Survey Digital Data Series 439, 1 CD-ROM, https://doi.org/10.3133/ds439.

Duffield, W.A., and Fournier, R.O., 1974, Reconnaissance study of the geothermal resources of Modoc county, California: U.S. Geological Survey Open-File Report 74-1024, 21 p., scale 1:250,000.

Dzurisin, D., Donnelly-Nolan, J.M., Evans, J.R., and Walter, S.R., 1991, Crustal subsidence, seismicity, and structure near Medicine Lake volcano, California: Journal of Geophysical Research, v. 96, p. 16,319–16,333.

Evans, J.R., and Zucca, J.J., 1988, Active high-resolution seismic tomography of compressional wave velocity and attenuation structure at Medicine Lake volcano, northern California Cascade Range: Journal of Geophysical Research, v. 93, p. 15016–15036.

Faulds, J.E., Henry, C.D., and Hinz, N.H., 2005, Kinematics of the northern Walker Lane—An incipient transform fault along the Pacific-North American plate boundary: Geology, v. 6, p. 505–508.

Finn, C., and Williams, D.L., 1982, Gravity evidence for a shallow intrusion under Medicine Lake volcano, California: Geology, v. 10, p. 503–507.

Finn, D.R., 1987, Geology and ore deposits of the Hayden Hill District, Lassen County, California: M.S. thesis, University of Nevada, Reno, 84 p.

Fraticelli, L.A., Albers, J.P., Irwin, W.P., Blake, M.C., Jr., and Wentworth, C.M., 2012, Digital geologic map of the Redding 1° x 2° quadrangle, Shasta, Tehama, Humboldt, and Trinity Counties, California: U.S. Geological Survey Open-File Report 2012-1228, scale 1:250,000, https://doi.org/10.3133/ofr20121228.

Fuis, G.S., Zucca, J.J., Mooney, W.D., and Milkereit, B., 1987, A geologic interpretation of seismic-refraction results in northeastern California: Geological Society of America Bulletin, v. 98, p. 53–65.

Gay, T.E., and Aune, Q.A., 1958, Geologic map of California—Alturas sheet: California Division of Mines and Geology, scale 1:250,000.

Glen, J.M.G., Egger, A.E., Ippolito, C., and Athens, N., 2013, Correlation of geothermal springs with sub-surface fault terminations revealed by high-resolution, UAV-acquired magnetic data, in Proceedings of the 38th Workshop on Geothermal Reservoir Engineering: Stanford Geothermal Program Workshop Report SGP-TR-198, p. 1233–1242.

Grauch, V.J.S., and Cordell, L., 1987, Limitations of determining density or magnetic boundaries from the horizontal gradient of gravity or pseudogravity data: Geophysics, v. 52, p. 118–121.

Grose, T.L., 2000, Volcanoes in the Susanville region, Lassen, Modoc, and Plumas Counties, northeastern California: California Geology, v. 53, p. 4–23.

Grose, T.L.T., Egger, A.E.., and O'Neal, M.D., 2016, Preliminary geologic map of the Alturas 30'×60' quadrangle, Lassen and Modoc counties, California: California Geological Survey, Preliminary Geologic Map, scale 1:100,000, 28 p., accessed December 29, 2021 at https://www.conservation.ca.gov/cgs/maps-data/rgm/preliminary.

Grose, T.L.T., Egger, A.E.., and O'Neal, M.D., 2017, Preliminary geologic map of the Cedarville 30'×60' quadrangle, Modoc county, California: California Geological Survey, Preliminary Geologic Map, scale 1:100,000, 22 p., accessed December 29, 2021 at https://www.conservation.ca.gov/cgs/maps-data/rgm/preliminary.

Grose, T.L.T., Saucedo, G.J., and Wagner, D.L., 2014a, Preliminary geologic map of the Eagle Lake 30'×60' quadrangle, Lassen county, California: California Geological Survey, Preliminary Geologic Map, scale 1:100,000, 35 p., accessed December 29, 2021 at https://www.conservation.ca.gov/cgs/maps-data/rgm/preliminary.

Grose, T.L.T., Saucedo, G.J., and Wagner, D.L., 2014b, Preliminary geologic map of the Susanville 30'×60' quadrangle, California: California Geological Survey, Preliminary Geologic Map, scale 1:100,000, 25 p., accessed December 29, 2021 at https://www.conservation.ca.gov/cgs/maps-data/rgm/preliminary.

Guffanti, M., Smith, J.G., Muffler, L.P.J., and Bullen, T.D., 1990, Late Cenozoic volcanism, subduction, and extension in the Lassen region of California, southern Cascade Range: Journal of Geophysical Research, v. 95, p. 19453–19464, https://doi.org/10.1029/JB095iB12p19453.

Hannah, J.L., 1977, Tectonic setting of the Modoc region, northeastern California, *in* Short contributions to California geology: California Division of Mines and Geology Special Report 129, p. 35–39.

Hart, W.K., Aronson, J.L., and Mertzman, S.A., 1984, Areal distribution and age of low-K, high-alumina olivine tholeiite magmatism in the northwestern Great Basin: Geological Society of America Bulletin, v. 95, p. 186–195.

Hazlett, D.P., 1984, A volcanotectonic and paleomagnetic investigation in the Hayden Hill area: M.S. thesis, Colorado School of Mines, 155 p.

Henry, C.D., Faulds, J.E., and dePolo, C.M., 2007, Geometry and timing of strike-slip and normal faults in the northern Walker Lane, northwestern Nevada and northeastern California: strain partitioning or sequential extensional and strike-slip deformation?, *in* Till, A.B., Roeske, S.M., Sample, J.C., and Foster, D.A., eds., Exhumation associated with continental strike-slip fault systems: Geological Society of America Special Paper 434, p. 59–79., https://doi.org/10.1130/2007.2434(04).

Hildreth, W., 2007, Quaternary magmatism in the Cascades—Geologic perspectives: U.S. Geological Survey Professional Paper 1359, 46 p.

Hill, P.L., Kucks, R.P., and Ravat, D., 2009, Aeromagnetic and aeroradiometric data for the conterminous United States and Alaska from the National Uranium Resource Evaluation Program of the U.S. Department of Energy: U.S. Geological Survey Open-File Report 2009–1129, https://doi.org/10.3133/ofr20091129.

Hulen, J.B., and Lutz, S.J., 1999, Altered volcanic rocks as hydrologic seals on the geothermal system of Medicine Lake volcano, California: Geothermal Resources Council Bulletin, v. 28, p. 217–222.

Irwin, W.P, 1994, Geologic map of the Klamath Mountains, California and Oregon: U.S. Geological Survey Miscellaneous Investigations Series Map I-2148, 2 pl., scale 1:500,000.

Jennings, C.W., Gutierrez, C., Bryant, W., Saucedo, G., and Wills, C., 2010, Geologic map of California: California Geological Survey, California Geological Survey Data Map 2, scale 1:750,000.

Kohler, W.M., Fuis, G.S., and Berge, P.A., 1987, Data report for the 1978-1985 seismic-refraction surveys in northeastern California: U.S. Geological Survey Open-File Report 87-625, 99 p.

Langel, R.A., 1992, International geomagnetic reference field—The sixth generation: Journal of Geomagnetism and Geoelectricity, v. 44, p. 679–707.

Langenheim, V.E., 2021, Aeromagnetic map of Burney and the surrounding areas, northeastern California: U.S. Geological Survey Open-File Report 2021-1006, scale 1:250,000, 8 p., https://doi.org/10.3133/ofr20211006.

Langenheim, V.E., 2022, Aeromagnetic Data of Alturas, California, and Surrounding Areas: U.S. Geological Survey data release, https://doi.org/10.5066/P9LU37RC.

Langenheim, V.E., 2023, Aeromagnetic and derivative gridded data, and magnetization boundaries of northeastern California: U.S. Geological data release, https://doi.org/10.5066/P9PUFYDD.

Langenheim, V.E., Jachens, R.C., Muffler, L.P.J., and Clynne, M.A., 2016, Implications for the structure of the Hat Creek graben and transfer of right-lateral shear from the Walker Lane north of Lassen Peak, northern California, from gravity and magnetic anomalies: Geosphere, v. 12, p. 790–808.

Langenheim, V.E., Ritzinger, B.T., Earney, T.E., Roberts, M.A., Chuchel, B.A., Sweetkind, D.S., and Sudman, B., 2019, Gravity and physical property data in the Chico and Willows 1:100,000-scale quadrangles, California: U.S. Geological Survey data release, https://doi.org/10.5066/P9B1O4TH.

Lerch, D.W., Klemperer, S.L., Glen, J.M.G., Ponce, D.A., Miller, E.L., and Colgan, J.P., 2007, Crustal structure of the northwestern Basin and Range province and its transition to unextended volcanic plateaus: G-cubed, v. 8, no. Q02011, 21 p., https://doi.org/10.1029/2006GC001429.

Lowenstern, J.B., Donnelly-Nolan, J.M., Wooden, J.L., and Charlier, B.L.A., 2003, Volcanism, plutonism and hydrothermal alteration at Medicine Lake volcano, California, Proceedings, Twenty-Eighth workshop on Geothermal Reservoir Engineering, Stanford, California, USA, January 27–29, 2003, http://ekofisk.stanford.edu/pdf/SGW/2003/Lowenstern.pdf

Luedke, R.G., and Smith, R.L., 1981, Map showing distribution, composition, and age of late Cenozoic volcanic centers in California and Nevada: U.S. Geological Survey Miscellaneous Investigations Map I–1091–C, scale 1:1,000,000, 2 sheets.

Lydon, P.A., Gay, T.E., Jr., and Jennings, C.W., compilers, 1960, Geologic map of California--Westwood sheet: California Division of Mines and Geology, scale 1:250,000.

McDonald, G.A., 1965, Geologic map of the Harvey Mountain quadrangle, Lassen County, California: U.S. Geological Survey Geologic Quadrangle GQ-443, scale 1:62,500; https://doi.org/10.3133/gq443.

Macdonald, G.A., 1966, Geology of the Cascade Range and Modoc Plateau, *in* Bailey, E.H., ed., Geology of northern California: California Division of Mines and Geology Bulletin, no. 190, p. 65–96.

McKee, E.H., Duffield, W.A., and Stern, R.J., 1983, Late Miocene and early Pliocene basaltic rocks and their implications for crustal structure, northeastern California and south-central Oregon: Geological Society of America Bulletin, v. 94, p. 292–304.

Meinzer, O.E., 1927, Large springs in the United States: U.S. Geological Survey Water-Supply Paper 557, 94 p.

Muffler, L.J.P., Clynne, M.A., and Champion, D.E., 1994, Late Quaternary normal faulting of the Hat Creek Basalt, northern California: Geological Society of America Bulletin, v. 106, p. 195–200.

Muffler, L.J.P., Robinson, J.E., Felger, T.J., Dutton, D.R., and Clynne, M.A., 2010, Database for the geologic map of Lassen Volcanic National Park and vicinity, California *in* Clynne, M.A., and Muffler, L.J.P., Geologic map of Lassen Volcanic National Park and vicinity: U.S. Geological Survey Scientific Investigations Map 2899, scale 1:50,000 [CD-ROM].

North American Magnetic Anomaly Group, 2002, Digital data grids for the magnetic anomaly map of North America: U.S. Geological Survey Open-File Report 02-0414, https://doi.org/10.3133/ofr02414.

Northern California Earthquake Data Center [NCEDC], 2014, Northern California Earthquake Data Center: Dataset, UC Berkeley Seismological Laboratory, accessed August 12, 2021, at https://doi.org/10.7932/NCEDC.

Ogg, J.G., 2020, Geomagnetic polarity timescale *in* Gradstein, F.M., Ogg, J.G., Schmitz, M.D., and Ogg, G.M., eds., The Geologic Time Scale 2020, vol. 1, Elsevier Publishing, Amsterdam, Netherlands, p. 159–192.

Pan-American Center for Earth and Environmental Studies, 2010, Gravity database, accessed January 8, 2010, http://cybershare.utep.edu/dataset/gravity-dataset-united-states-lower-48-states.

Phillips, J.D., 2001, Designing matched bandpass and azimuthal filters for the separation of potential-field anomalies by source region and source type: Australian Society of Exploration Geophysicists, 15th Geophysical Conference and Exhibition, Expanded Abstracts CD-ROM, 4 p.

Poland, M., Burgmann, R., Dzurisin, D., Lisowski, M., Masterlark, T., Owen, S., and Fink, J., 2006, Constraints on the mechanism of long-term, steady subsidence at Medicine Lake volcano, northern California, from GPS, leveling, and InSAR: Journal of Volcanology and Geothermal Research, v. 150, p. 55–78.

Ramsey, D.W., Felger, T.J., Lougee, Ellen, Bruggman, P.E., and Donnelly-Nolan, J.M., 2010, Database for the geologic map of Medicine Lake volcano, northern California, *in* Donnelly-Nolan, J.M., Geologic map of Medicine Lake volcano, northern California: U.S. Geological Survey Scientific Investigations Map 2927 [CD-ROM]

Sawyer, T.L., and Bryant, W.A., compilers, 1995, Fault number 5, Likely fault zone, in Quaternary fault and fold database of the United States: U.S. Geological Survey website, accessed December 14, 2020 at https://earthquake.usgs.gov/cfusion/qfault/show_report_AB_archive.cfm?fault_id=5&section_id=.

Sherrod, D.R., and Keith, M.K., 2018, GIS database and discussion for the distribution, composition, and age of Cenozoic volcanic rocks of the Pacific Northwest Volcanic Aquifer System study area: U.S. Geological Survey Open-File Report 2018–1030, 16 p., https://doi.org/10.3133/ofr20181030.

Stanley, W.D., Mooney, W.D., and Fuis, G.S., 1990, Deep crustal structure of the Cascade Range and surrounding regions from seismic refraction and magnetotelluric data: Journal of Geophysical Research, v. 95, p. 19419–19438.

Sweetkind, D.S., and Langenheim, V.E., 2022, Data release of Geologic data for the Aeromagnetic Map of Northeastern California: U.S. Geological Survey data release, https://doi.org/10.5066/P91Y9L0H.

Turrin, B.D., Christiansen, R.L., Clynne, M.A., and 4 others, 1998, Age of Lassen Peak, California, and implications for the ages of late Pleistocene glaciations in the southern Cascade Range: Geological Society of America Bulletin, v. 110, p. 931–945.

Unruh, J., and Humphrey, J., 2017, Seismogenic deformation between the Sierran microplate and Oregon coast block: Geology, v. 45, p. 415–418, https://doi.org/10.1130/G38696.1.

Unruh, J., Humphrey, J., and Barron, A., 2003, Transtensional model for the Sierra Nevada frontal fault system, eastern California: Geology, v. 31, p. 327–330, https://doi.org/10.1130/0091-7613(2003)031%3C0327:TMFTSN%3E2.0.CO;2.

U.S. Geological Survey, 2019, The National Map, accessed February 15, 2019, at https://apps.nationalmap.gov/viewer/.

U.S. Geological Survey and California Geological Survey, 2006, Quaternary fault and fold database for the United States: U.S. Geological Survey website, accessed February 22, 2012, at https://doi.org/10.5066/F7S75FJM.

Waldien, T.S., Meigs, A.J., and Madin, I.P., 2019, Active dextral strike-slip faulting records termination of the Walker Lane belt at the southern Cascade arc in the Klamath graben, Oregon, USA: Geosphere, v. 15, no. 3, p. 882–900, https://doi.org/10.1130/GES02043.1.

Wang, X., and Hansen, R.O., 1990, Inversion for magnetic anomalies of arbitrary three-dimensional bodies: Geophysics, v. 55, p. 1321–1326.

Wesnousky, S.G., 2005, The San Andreas and Walker Lane fault systems, western North America—Transpression, transtension, cumulative slip and the structural evolution of a major transform plate boundary: Journal of Structural Geology, v. 27, p. 1505–1512.

Zohdy, A., and Bisdorf, R.J., 1990, Schlumberger soundings near Medicine Lake, California: Geophysics, v. 55, p. 956–964.

Zucca, J.J., Fuis, G.S., Milkereit, B., Mooney, W.D., and Catchings, R.D., 1986, Crustal structure of northeastern California: Journal of Geophysical Research, v. 91, p. 7359–7382.